

**THE UNIVERSITY OF ARIZONA,**  
**DEPARTMENT OF GEOSCIENCES**

Geosciences Dept.  
University of Arizona  
1040 E. Fourth St.  
Tucson, AZ 85721  
April 12, 2016

Dear Editor:

Please consider our updated manuscript for acceptance. We wish to thank the two reviewers for their helpful reviews that have led us to improve the paper. Below is a point-by-point discussion of the changes we have made to address the comments from both reviewers. We have also provided a “tracked-changes” draft of the main body of the paper and the three updated figures following this discussion.

**General Comment**

In our paper we extended the concept of the flood-envelope curve (a common technique to estimate the maximum-probable flood for ungaged drainage basins) to include event probability or recurrence interval explicitly. The reviewer counters that we neglected many of the known controls on discharge in our model framework. We accept his/her point but we wish to note that methods for predicting peak discharges come in many different forms with many different levels of complexity. On the simplest end of the spectrum are models that relate peak discharge to drainage area alone. These methods include the flood-envelope curve and related regional fits of peak discharge data to drainage area. Such methods neglect many known controls on discharge but they are not “wrong.” Rather, they capture the first-order control on peak discharge and have the advantage of requiring very little input data (this is an advantage because more sophisticated models with more parameters are not necessarily superior, i.e. they can be overfit). Our goal was to develop a method for predicting peak discharges that retains the simplicity of the flood-envelope curve yet allows for variable recurrence intervals. As such, while the reviewer is correct that many dozens of variables control the hydrological response of watersheds, we dispute the suggestion that all hydrology studies must explicitly include all known controls. We believe that the simplifications we have made are appropriate within the context of the goal of our project, which was to generalize the flood-envelope-curve approach to variable recurrence intervals and to understand the first-order controls on the shape of frequency-magnitude-area plots of peak discharge.

**Reviewer 1**

**Hydrology Questions/Comments**

**Q1) The estimation of the losses via a runoff coefficient computed elsewhere is a significant assumption that requires validation in real watersheds of the study area (see also point 3) by comparison with observed discharge. Since the authors have used real precipitation events and not synthetic ones, this could be done. As it is, I**

**have very little confidence in the results of the methodology (even if they may be correct).**

A) We chose to use two existing studies to estimate the runoff coefficients for our model drainage basins, one of which is, in fact, based on our study area. The runoff coefficient was estimated using Vivoni et al. (2007) for smaller basins (less than  $10^3$  km<sup>2</sup>) and Rosenberg et al. (2013) for larger basins.

The data for small basins comes from a model applied to a basin in Oklahoma with runoff coefficients calculated for wet, medium, and dry conditions. Not only is this one of the few studies that report runoff coefficients for such small drainage basins, it is the only study that we are aware of that reports runoff coefficients for a range of antecedent moisture conditions. Antecedent moisture conditions are undoubtedly important for hydrologic response yet are non-trivial to constrain or specify in a way that does not involve a large number of poorly constrained parameters. Runoff-coefficient data from real drainage basins of the size considered by the Vivoni et al. (2007) study simply are not available within the CRB for the range of antecedent moisture conditions.

The data for large basins comes from the aggregated annual runoff coefficients calculated for basins within our study area in the CRB. These values are directly applicable to our study areas. The use of the previously published runoff coefficients is supported by the resulting relationships between basin area and runoff coefficients that show the expected pattern with wet, medium, and dry conditions causing high, medium, and low runoff coefficients.

Although we have real precipitation data from the CRB, modeling runoff coefficients for specific basins in the CRB was not within the scope of this paper (i.e. we did not use precipitation data in a detailed way, i.e. relating it to one specific basin area) and would warrant another study altogether in order to get a representative value. This second study would need to be a regional assessment type study that is similar in size and scope to those studies and reports we used in order to find channel slope data for the CRB.

Our methods in this study are simplified relative to detailed process-based drainage basin hydrologic models, but this was by design. We believe our simplified approach is warranted by the fact that the end goal of the study is to quantify and predict the effects of basin area on peak discharges within a given region in order to provide a tool for quickly estimating the recurrence intervals of extreme floods in ungaged drainage basins using area as the sole required input parameter.

**Q2) It is not clear how the runoff coefficient is included in the calculations and the symbols and equations introduced never mentioned.**

A) The runoff coefficients were used to remove a volume of water before the water volume was distributed and routed through the model drainage basin. This was done for the three moisture conditions separately (results shown in Fig. 7). This was described in the text, but not shown mathematically. An equation and text describing this step of the analysis has been added:

“The flow-routing algorithm we employ does not explicitly include infiltration and other losses that can further reduce  $Q_{fd}$  relative to  $Q_p$ . In this study we modeled infiltration and evaporation losses by simply removing a volume of water per unit time

equal to one minus the runoff coefficient, i.e. the ratio of runoff to precipitation over a specified time interval, for three antecedent-moisture scenarios (wet, med, and dry). We estimated runoff coefficients for each contributing-area class and each of three antecedent-moisture scenarios using published values for annual runoff coefficients for large basins within the UCRB and LCRB (Rosenburg et al., 2013) and published values for event-based runoff coefficients for small basins modeled with a range of antecedent-moisture conditions by Vivoni et al. (2007) (Fig. 3). On average, estimated runoff coefficients are higher for smaller and/or initially wetter basins. We found the dependence of runoff coefficients on contributing area and antecedent moisture to be similar despite the large difference in time scales between event-based and annual values. Despite the difference in geographic region between our study site and that of Vivoni et al. (2007) (they studied basins in Oklahoma), the runoff coefficients they estimated are likely to be broadly applicable to the LCRB and UCRB given that basin size and antecedent moisture are the primary controls on these values (climate and soil types play a lesser role except for extreme cases).

We applied the estimated runoff coefficients for all three antecedent-moisture scenarios by simply using them to remove a portion of the  $Q_p$  calculated for specific time interval and basin area

$$Q_{pm} = C * Q_p$$

where  $C$  is the runoff coefficient calculated for the specific basin area and antecedent-moisture scenario under evaluation. The newly formed  $Q_{pm}$  is now the  $Q_p$  value for the wet, medium, or dry antecedent-moisture scenario under analysis.”

“The assigned channel slope and width values, together with the values of  $Q_{pm}$  modified for each antecedent-moisture scenario, were used to calculate the depth-average velocities,  $V$  ( $m s^{-1}$ ), in hypothetical 1D main-stem channels of idealized square drainage basins corresponding to each contributing-area and time-interval-of-measurement class. In this study, flow velocity is not modeled over space and time, but rather is set at a constant value appropriate for the peak discharge using an iterative approach that solves for the peak depth-averaged flow velocity, uses that velocity to compute the parameters of the diffusion-wave-routing algorithm, routes the flow, and then computes an updated estimate of peak depth-averaged velocity.”

**Q3) How are the wet, medium, and dry conditions taken into account? This was not explicitly described.**

A) Please see above.

**Q4) The same problem applies for the assumption of a triangular shape of the transfer function: it requires validation.**

A) We are aware that basin size, shape, and the topology of the stream network can affect flood magnitudes. However, in this study we chose to avoid such basin-specific characteristics in order to seek a more general understanding and prediction of how event discharges scale with drainage area. We chose to use a triangular basin area function on the basis of the fact that the average basin area and/or width function has been found to

be approximately triangular based on many previous studies (Marani et al., 1994; Rinaldo et al., 1995; Veneziano et al., 2000; Rodriguez-Iturbe and Rinaldo, 2001; Puente and Sivakumar, 2003; Saco and Kumar, 2008; Rigon et al., 2011). Using a triangular basin area function gives us a smooth and simplified representation of real basins without including the unique individual noise of a specific basin. A future study in this area could be the effect of the shape of the basin width function on the peak flood magnitude as well as other discharge characteristics. Text and additional references concerning this assumption have been added:

“The flow-routing algorithm routes flow along the main-stem channel of idealized square basins with sizes equal to the contributing area of each contributing-area class. The choice of a square basin is consistent with the square sample areas (see Section 3.1) and it allows for basin shape to remain the same (and therefore comparable) over the range of contributing areas used in this study. The main-stem channel, with a length of  $L$  (m), was defined as the diagonal distance from one corner to the opposite corner across the square basin (i.e.  $L$  is equal to the square root of two times the area of the square basin). This main-stem channel was used in conjunction with a normalized area function to represent the shape of the basin and the routing of runoff through the drainage basin network. By including the normalized area function, we can account for geomorphic dispersion (i.e. the attenuation of the flood peak due to the fact that precipitation that falls on the landscape will take different paths to the outlet and hence reach the outlet at different times) in our analyses. The normalized area function,  $A(x)$  (unitless), is defined as the portion of basin area,  $A_L(x)$  ( $m^2$ ), that contributes flow to the main-stem channel within a given range of distances ( $x$ ) from the outlet, normalized by the total basin area,  $A_T$  ( $m^2$ ; Mesa and Mifflin, 1986; Moussa, 2008). The normalized area function is assumed to be triangular in shape with a maximum value at the midpoint of the main-stem channel from the outlet. Area functions, and related width functions, from real basins used in other studies show this triangular shape in general (Marani et al., 1994; Rinaldo et al., 1995; Veneziano et al., 2000; Rodriguez-Iturbe and Rinaldo, 2001; Puente and Sivakumar, 2003; Saco and Kumar, 2008), although not all basins show this shape. The triangular area function has been shown to approximate the average area function of basins and that the peak discharge and time to peak discharge is likely more important to the shape of the flood wave (Henderson, 1963; Rodriguez-Iturbe and Valdes, 1979).”

Henderson, F.M.: Some properties of the unit hydrograph, *J. Geophys. Res.*, 68, 4785-4793, 1963.

Marani, M., Rinaldo, A., Rigon, R., Rodriguez-Iturbe, I.: Geomorphological width functions and the random cascade, *Geophys. Res. Lett.*, 21, 2123-2126, 1994.

Puente, C.E. and Sivakumar, B.: A deterministic width function model, *Nonlinear Proc. Geoph.*, 10, 525-529, 2004.

Rinaldo, A., Vogel, G.K., Rigon, R., Rodriguez-Iturbe, I.: Can one gauge the shape of a basin?, *Water Resour. Res.*, 31, 1119-1127, 1995.

Veneziano, D., Moglen, G.E., Furcolo, P., Iacobellis, V.: Stochastic model of the width function, *Water Resour. Res.*, 36, 1143-1157, 2000.

**Q5) The only validation performed is against the FEC curves published for LCRB and U.S., which are based on observed discharges, after post-processing the results via the frequency analysis. Figure 7 shows significant differences (the axis is logarithmic) between the FEC curves and those generated via the FMA method, which are based on observed precipitation. The authors have not explained the reasons of these discrepancies and it is hard to have confidence on these results, especially considering the potential use of these curves for flood-related management and design purposes.**

A) It is incorrect to state that the comparison of the FMACs to the published FECs is a validation. These curves are very different and there is no reason to expect that they should match. First, the data used to create each curve are not the same (i.e. FMACs use our rainfall-runoff model-derived flood values while FECs use measured floods from the record). Second, we did not expect the FMACs to match the U.S. FEC in magnitude (and possibly even in shape) because of the variation in types of storms and flooding associated with the U.S. FEC (especially larger extreme forcings like hurricanes) that are not included within the data for the UCRB and LCRB. However, we did expect to see generally similar shapes and/or order of magnitudes between the FMACs and FECs for the LCRB because they are the same hydroclimatic region. There are discrepancies between the two curves, but exact reasons between the discrepancies are very difficult to determine when using a simplified model approach and would need to be addressed using a model that included and tested those variables. Lastly, one of the motivations for creating a new method is that we feel that the FEC curve is biased towards underestimating the size of large floods in larger drainage basins. The FEC curve is defined by the largest flood, and since there are many more small drainage basins within any hydroclimatic region than large drainage basins, it is likely that the maximum flood for the smaller drainage basins will represent a more extreme (i.e. high recurrence interval or low flow duration) event. Our method corrects for this bias.

**Q6) Why have not the authors considered real basins with real stream networks? The basin shape (that affects the rainfall effectively fallen in the basin) and the stream network organization are known to have critical importance on the flood timing and magnitude.**

A) We are aware that the individual basin shape and stream network are an integral part in understanding flood size, timing, and nature. Again, this paper is looking for regional trends in flood size and frequency and how they scale with drainage basin area. This approach was motivated by the history of predicting peak flood discharges from simple variables, such as basin area. Moreover, it would have been difficult or impossible to aggregate different basins together within a space-for-time substitution (in which subbasins within a given hydroclimatic regime provide replicates of each other than allow extreme floods to be estimated from a relatively short record) without subdividing each large basin into equal size smaller basins as we did. That aggregation is central to the whole idea and it would have been much more difficult if subdivided the watersheds into non-equal areas.

**Q7) Given the simplified nature of the method, no contribution of snow and snowmelt was considered. This has to be stated. Regarding the snow contribution, I**

**have also doubts about what has been stated on p. 11759, line 28, and p. 11760, line 1: are the authors assuming that NEXRAD products provide snowfall (which they don't)?**

A) We agree that the exclusion of snow effects and the focus on rainfall-generated floods was not stated clearly. In the revised paper we have modified the discussion of the NEXRAD processing and the title of the paper to make clear that we are considering rainfall-triggered floods only (i.e. not snowmelt floods or rain-on-snow floods). On the lines pointed out by the reviewer, we explain that the NEXRAD data likely does include some snowfall measurements. These snowfall measurements, as stated in the discussion, would be identified by the NEXRAD processing as a low-intensity precipitation event. However, in this study we are only interested in the maximum precipitation intensity and therefore these values would effectively be ignored. We should also note that we choose to work on the Colorado River Basin in part because snowmelt-induced flooding is expected to be the dominant cause of flooding for only a small portion of these watersheds (e.g. Niezgodna and West, 2012, relate the predominance of snowmelt-induced flooding to the portion of drainage basins above 9000 ft in elevation in the western U.S.). We don't think this limitation negatively impacts the importance of our work for rainfall-generated floods.

Changes to the title and the text are as follows:

“Constraining frequency-magnitude-area relationships for rainfall and flood discharges using radar-derived precipitation estimates: Example applications in the Upper and Lower Colorado River Basins, USA”

“In this study, a new method for estimating flood discharges associated with user-specified recurrence intervals is introduced that uses radar-derived precipitation estimates (in this case rainfall only), combined with the diffusion-wave flow-routing algorithm, to create frequency-magnitude-area curves (FMACs) of flood discharge. Our method (i.e. the FMAC method) retains the power of the FEC approach in that data from different drainage basins within a hydroclimatic region are aggregated by contributing area, thereby enabling large sample sizes to be obtained within each contributing-area class in order to more accurately constrain the frequencies of past extreme flood events and hence the probabilities of future extreme flood events within each class. The method improves upon the FEC approach in that the complete spatial coverage of radar-derived precipitation estimates provides for large sample sizes of most classes of contributing area (larger contributing areas have fewer samples). The radar-derived precipitation estimates include only rainfall and therefore snow and other types of precipitation are not included in the study. The precipitation estimates are then used to predict flood discharges associated with specific recurrence intervals by first accounting for water lost to infiltration and evapotranspiration using runoff coefficients appropriate for different contributing areas and antecedent-moisture conditions, and then routing the available water using a flow-routing algorithm. Predicted flood discharges are presented as FMACs on log-log plots, similar to traditional FECs, except that the method predicts a family of curves, one for each user-defined recurrence interval. These plots are then compared to FECs for the study region (Enzel et al., 1993) and the U.S. (Costa, 1987).”

“Under- and over-estimation of precipitation by NEXRAD products in relation to rain-gauge data is partly due to the difference in sampling between areal NEXRAD products and point data from rain gauges and partly due to sampling errors inherent to both methods. For example, NEXRAD products include problems such as the use of incorrect Z-R relationships for high intensity storms and different types of precipitation, such as snow and hail (Baeck and Smith, 1998). Also, because of its low reflectivity, snow in the NEXRAD products is measured as if it were light rain (David Kitzmiller, personal communication, January 10, 2012). This means the NEXRAD products likely underestimate snowfall and therefore snowfall is not fully accounted for in this study. Due to snowfall not being included in this study, associated snowpack and snowmelt effects were also not accounted for. Rain gauges can also suffer from a number of measurement errors that usually result in an underestimation of rainfall (Burton and Pitt, 2001). In addition, gridded rainfall data derived from rain gauges are not spatially complete and therefore must be interpolated between point measurements to form a spatially complete model of rainfall. It is impossible to discern which product is more correct due to the differences in measurement techniques and errors, but by taking both products and combining them into one, the Stage III NEXRAD precipitation products generate the best precipitation estimate possible for this study. Moreover, it should be noted that 100-year flood magnitude predictions based on regression equations have very large relative error bars (ranging between 37 to 120% in the western U.S.; Parrett and Johnson, 2003) and that measurements of past extreme floods can have significant errors ranging from 25% to 130% depending on the method used (Baker, 1987). As such, even a ~50% bias in NEXRAD-product-derived precipitation estimates is on par or smaller than the uncertainty associated with an analysis of extreme flood events.”

“As stated previously, the NEXRAD precipitation estimates used here do not include snowfall and other non-rainfall precipitation types. In this study we also do not include snowpack information into our flood discharge calculations. The omission of snowpack is a reasonable assumption for our low elevation, warm regions within most of the UCRB and LCRB. However, we acknowledge some of our higher elevation areas at higher latitudes may be underestimating the maximum flood discharge by only including rainfall-derived runoff. If the methodology in this paper were applied to a snowmelt-dominated region, snowpack would need to be added to accurately estimate the maximum flood discharge.”

Niezgoda, S. and West, T. (2012) Relationships between Watershed and Stream Characteristics and Channel Forming Discharge in Snowmelt Dominated Streams. World Environmental and Water Resources Congress 2012: pp. 1575-1584.  
doi: 10.1061/9780784412312.157

**Q8) The description of the methodology is not complete and some details not well explained. I think that more symbols and equations should be introduced to explain better each step, along with a figure that shows a schematic of the approach and an example of a basin (I found Fig. 2 not informative at all).**

A) We have added to the description of the methodology and equations based on the other points brought up in this review. A schematic flow chart of the steps within the methods has been added below, please let us know if the schematic is helpful.

“Figure #. Schematic diagram of methodology used in this paper. (A) Rainfall data is sampled over spatial and temporal scales in factors of two. This sampling does not only include looking at the data within a given spatial or temporal scale, but aggregating it over that scale. These values are ranked for a given basin area and time interval to complete the frequency analysis. This results in rainfall intensities ( $I$ ) for each spatial scale (basin area), temporal scale (time interval or storm duration), and frequency. (B) Intensities sampled from the rainfall data are used to calculate rainfall discharge ( $Q_p$  and  $Q_{pm}$ ) values that are then put through the flow routing algorithm in order to calculate flood discharge ( $Q_{fd}$ ) values.  $Q_{fd}$  values are then used to construct the frequency-magnitude-area curves (FMACs) showing the data for recurrence intervals of 10, 50, 100, and 500 years.”

### **Frequency Estimation Questions/Comments**

**Q9) In extreme value theory, recurrence intervals are calculated for independent events, either deriving annual maxima or through the peak over threshold approach. In both cases, a time series of a variable observed at a location or a basin is used. In the paper under review, the computation of the recurrence interval accounts for all events observed in all basins of the same drainage area. Assuming that we have  $N$  basins with the same area (e.g. 64 km<sup>2</sup>) included in the Upper and Lower CRBs, this implies that the recurrence interval is calculated by pooling together  $N$  time series of a variable. Through this method, the authors could present discharge values for the 500-year return period, using 10 years of rainfall records. However, since storms may have happened at the same time in contiguous basins, the events may not be statistically independent, as they are originated from the same weather pattern. In other words, increasing the sample size with records of contiguous basins is not a trivial operation, which requires careful evaluation. This may contradict the principle of extreme value theory. Addressing this issue is crucial to build FMA curves and the authors have not provided any justification.**

A) We are aware that extreme value theory requires that values within the distribution be statistically independent of one another. The reviewer’s comments have inspired us to check our calculations and check that our methods are consistent with the peak over threshold method. We have made a few minor changes to our code that make sure we identify the peak discharge associated with rainfall events (associated with the peak intensities of individual rainfall events) of a given recurrence interval without double counting. We specify a threshold value of zero and use it to identify individual storm events in our data, i.e. storm events are identified by adjacent strings of intensity values above zero separated from other strings of intensity values by zeros.

In this method we also consider a range of possible storm durations to arrive at the peak rainfall intensities and associated discharges for a given sized watershed. However, the main purpose of specifying a threshold in the peak-over-threshold approach is to avoid “double counting,” i.e. counting multiple peaks of a single flood event as two



or more separate events. Our routing method, which uses a triangular width function and assumes constant rainfall over the duration of the storm, produces a single peak in the hydrograph. As such, there is no possibility of double counting, i.e. there is a single peak discharge associated with each rainfall event.

The minor changes to the code have changed some of our values, but only slightly. That is, those intensity, precipitation discharge, and flood discharges that have changed only changed by a very small amount, keeping the trends and conclusions in our paper the same. The largest changes were those of the errors, which in general increased slightly based on the fact that there are larger differences between the value so the specified ranks and those at the next highest rank. This is to be expected since our minor changes resulted in less duplicates and less samples overall. Changes to the text (mostly the power-law fits), tables (both tables 1 and 2), and figures (figures 6 and 7) have been incorporated. Please see marked copy of manuscript.

**Q10) Additionally, in the case of precipitation, a fixed duration is utilized in extreme value theory to compute the recurrence interval (e.g. the 100 year rainfall intensity for 1-h duration). In this paper, the authors find the maximum intensity recorded for different aggregations times, chosen arbitrarily. This choice has to be supported as well.**

**A)** The time intervals used to integrate the precipitation data were not chosen arbitrarily. We chose to use time intervals of powers of 2 to simplify the approach and to incorporate a range of time intervals from 1 hour to 64 hours. As stated in the text, this range was chosen to include short-duration precipitation events such as convective-type and/or monsoon storms (typically high intensity, short duration summer storms in the UCRB and LCRB) and long-duration precipitation events that last on the order of days such as frontal-type storms (typically lower intensity, long duration winter storms in the UCRB and LCRB). It is important to note as well that the highest maximum precipitation intensities for a given basin area (the main focus of this study) were found during smaller time intervals, so including even one larger time interval would not change the results of this study.

## **Reviewer 2**

**Q1) The authors make a strong case in the introduction about the need to incorporate recurrence intervals to the FEC methodology. However, they do not indicate that to some extent, this has already been done. The work by Castellarin et al. (2005, 2007, 2009), which is mentioned in point 5.2 should be included in the introduction to show the real state of the art. As it is now, the only papers that are mentioned in the intro are more than 10 yrs old and it looks like nobody has done anything on the subject since then. Section 5.2 should be moved to the intro as it also does not belong in the discussion (too general and without any quantitative support). This may require some rewording and a clearer statement about the novelty of the current application.**

**A)** We have accepted this suggestion by Reviewer 1 and moved section 5.2 to the introduction. This portion of the introduction now states:

“Traditional FECs also have the potential problem that the maximum flood associated with smaller drainage basins may be biased upward (or the floods of larger drainage basins biased downward) because there are typically many more records of floods in smaller drainage basins relative to larger drainage basins (because there are necessarily fewer large drainage basins in any hydroclimatic region). That is, the largest flood of record for small drainage basins within a hydroclimatic region likely corresponds to a flood of a larger recurrence interval compared with the largest flood of record for larger drainage basins. In this paper we present a method that includes recurrence-interval information and avoids any sample-size bias that might exist as a function of contributing area.

The use of FECs to quantify flood regimes is limited by the lack of recurrence-interval information (Wolman and Costa, 1984; Castellarin et al., 2005) and by the short length, incomplete nature, and sparseness of many flood-discharge records. Without recurrence-interval information, the data provided by FECs are difficult to apply to some research and planning questions related to floods. In the U.S. for example, the 100- and 500-year flood events are the standard event sizes that define flood risk for land planning and engineering applications (FEMA, 2001).

Previously published studies have looked at new approaches to approve upon the FEC method. Castellarin et al. (2005) took a probabilistic approach to estimating the exceedance probability of the FEC for synthetic flood data. The authors were able to relate the FECs of certain recurrence intervals to the correlation between sites, the number of flood observations, and the length of each observation. Later, Castellarin (2007) and Castellarin et al. (2009) applied these methods to real flood record data and extreme rainfall events for basins within north-central Italy. Castellarin et al. (2009) also created depth-duration envelope curves of precipitation to relate extreme precipitation events to mean annual precipitation. This group of studies was successful in incorporating recurrence-interval information into the traditional FEC method. However, most of the models presented in these studies were completed with synthetic data or created for design storm processes and require additional analysis. Also, most of the precipitation data used in these past studies was collected using rain gauges (point sources), while only a small subset of data in Castellarin et al. (2009) was sourced from radar-derived precipitation estimates. In contrast to these studies we formulate a simplified method (i.e. the FMAC method) that is readily applicable to any region of interest and can be directly compared to already existing FECs. Also we favor the use of spatially complete radar-derived precipitation estimates in order to apply our methods to ungauged basins.”

**Q2) The methodology has a number of assumptions and simplifications that are not always thoroughly justified or tested. Since the final model results are not really suitable for a validation, more emphasis should be put into the individual components of the methodology to convince the reader of the validity of the results.**

Please see the above comments from Reviewer 1 in which we have responded to specific concerns about certain assumptions and variables. Please let us know if there are other locations that require additional attention.

**Q3) Regarding the last point, the selection of runoff coefficients needs a lot more justification. Figure 3 does not do a good job in convincing readers of a sensible methodology. The determination of the wet, dry and intermediate antecedent conditions runoff coefficients does not agree with the data very much, and may question the assumption that such simple separation is meaningful. For example, half of the dry data of Vivoni et al. (2007) is better described by the intermediate curve, and the same goes for half of the intermediate data that falls close to the wet curve. There is also no mention of the antecedent conditions of the Rosenberg et al. 2013 data. I would also argue that the Rosenberg data does not show any dependence of the runoff coefficient with contributing area. This poor agreement with the data is reflected by the low correlation coefficient, particularly for the dry antecedent conditions (0.04). The authors should justify the validity of the runoff coefficients, and also perform a sensitivity analysis. This is particularly important since the uncertainty analysis of 3.4 does not include parameter uncertainty.**

The trend lines shown in Figure 3 were found as average trends of runoff coefficients with contributing area. The data from Vivoni et al. (2007) does vary for the dry and intermediate antecedent moisture conditions, but this is due to the length and intensity of the storm used to calculate those runoff coefficients and is interpreted as showing the low and high end of possible runoff coefficients under those antecedent moisture conditions. We chose to fit a trendline to the data including both the low and high end to get an average runoff coefficient relationship to contributing area with the understanding that the trendline may have a low correlation coefficient. We feel that this is warranted based on the lack of runoff coefficient data in the literature that includes antecedent moisture data (Vivoni et al.'s study was the only study to have this type of data that the authors know of) and the uncertainty associated with the broad drainage-basin-wide conditions this study includes that affect runoff coefficients. The Rosenberg data is the only runoff coefficient data we found for our study area and no antecedent moisture conditions were given for the data. This is understandable due to the large areas and yearly time frame over which these runoff coefficients were calculated. The Rosenberg data is also just a small sample of the many basins in the CRB and may therefore not show a clear dependence with contributing area. However, we would argue that the data do show that for larger drainage basins ( $>10^3$  km<sup>2</sup>) the runoff coefficients are less than 0.4, which constrains our trend lines to a lower runoff coefficient for larger basins than smaller basins. This constraint leaves a trendline with a predictable relationship of higher runoff coefficients occurring in smaller drainage basins.

Overall, it is unfortunate that a national assessment of runoff coefficients for each hydroclimatic region does not exist. This sort of study would need to use rainfall data (NEXRAD data or similar), soil moisture data (possibly from the NCEP reanalysis), and discharge data (USGS gages or similar) for available basins to calculate a runoff coefficient. This would be very helpful for many hydrologic and ecological studies. In the end we felt that this type of study was beyond the scope of our study and chose to rely on previously published studies for runoff coefficient information.

Thank you,

A handwritten signature in black ink that reads "Caitlin A. Orem". The signature is written in a cursive style with a large initial "C".

Caitlin A. Orem, [oremc@email.arizona.edu](mailto:oremc@email.arizona.edu)

A handwritten signature in black ink that reads "Jon D. Pelletier". The signature is written in a cursive style with a large initial "J".

Jon D. Pelletier, Professor, [jdpellet@email.arizona.edu](mailto:jdpellet@email.arizona.edu)

1 | **Constraining frequency-magnitude-area relationships for rainfall and flood**  
2 | **discharges using radar-derived precipitation estimates: Example applications in the**  
3 | **Upper and Lower Colorado River Basins, U.S.A.**

4 | Caitlin A. Orem\*, Jon D. Pelletier

5 | [1] {Department of Geosciences, The University of Arizona, 1040 E. 4<sup>th</sup> Street, Tucson,  
6 | AZ 85721, USA}

7 | Correspondence to: C.A. Orem (oremc@email.arizona.edu)

8 |  
9 | **Abstract**

10 | Flood-envelope curves (FEC) are useful for constraining the upper limit of possible flood  
11 | discharges within drainage basins in a particular hydroclimatic region. Their usefulness,  
12 | however, is limited by their lack of a well-defined recurrence interval. In this study we  
13 | use radar-derived precipitation estimates to develop an alternative to the FEC method, i.e.  
14 | the frequency-magnitude-area-curve (FMAC) method, that incorporates recurrence  
15 | intervals. The FMAC method is demonstrated in two well-studied U.S. drainage basins,  
16 | i.e. the Upper and Lower Colorado River basins (UCRB and LCRB, respectively), using  
17 | Stage III Next-Generation-Radar (NEXRAD) gridded products and the diffusion-wave  
18 | flow-routing algorithm. The FMAC method can be applied worldwide using any radar-  
19 | derived precipitation estimates. In the FMAC method, idealized basins of similar  
20 | contributing area are grouped together for frequency-magnitude analysis of precipitation  
21 | intensity. These data are then routed through the idealized drainage basins of different  
22 | contributing areas, using contributing-area-specific estimates for channel slope and  
23 | channel width. Our results show that FMACs of precipitation discharge are power-law  
24 | functions of contributing area with an average exponent of  $0.82 \pm 0.06$  for recurrence  
25 | intervals from 10 to 500 years. We compare our FMACs to published FECs and find that  
26 | for wet antecedent-moisture conditions, the 500-year FMAC of flood discharge in the  
27 | UCRB is on par with the U.S. FEC for contributing areas of  $\sim 10^2$  to  $10^3$  km<sup>2</sup>. FMACs of  
28 | flood discharge for the LCRB exceed the published FEC for the LCRB for contributing  
29 | areas in the range of  $\sim 10^3$  to  $10^4$  km<sup>2</sup>. The FMAC method retains the power of the FEC  
30 | method for constraining flood hazards in basins that are ungauged or have short flood

31 records, yet it has the added advantage that it includes recurrence interval information  
32 necessary for estimating event probabilities.

33

## 34 **1. Introduction**

### 35 **1.1 Flood-Envelope Curves**

36 For nearly a century, the flood-envelope curves (FEC), i.e. a curve drawn slightly  
37 above the largest measured flood discharges on a plot of discharge versus contributing  
38 area for a given hydroclimatic region (Enzel et al., 1993), have been an important tool for  
39 predicting the magnitude of potential future floods, especially in regions with limited  
40 stream-gauge data. FECs assume that, within a given hydroclimatic region, maximum  
41 flood discharges for one drainage basin are similar to those of other drainage basins of  
42 the same area, despite differences in relief, soil characteristics, slope aspect, etc. (Enzel et  
43 al., 1993). This assumption enables sparse and/or short-duration flood records over a  
44 hydroclimatic region to be aggregated in order to provide more precise constraints on the  
45 magnitude of the largest possible (i.e. long-recurrence-interval) floods.

46 FECs reported in the literature have a broadly similar shape across regions of  
47 widely differing climate and topography. For example, FECs for the Colorado River  
48 Basin (Enzel et al., 1993), the central Appalachian Mountains (Miller, 1990; Morrison  
49 and Smith, 2002), the 17 hydrologic regions within the U.S. defined by Crippen and Bue  
50 (1977), the U.S. as a whole (Costa, 1987; Herschy, 2002), and China (Herschy, 2002) are  
51 all concave-down when plotted in log-log space, with maximum recorded flood  
52 discharges following a power-law function of contributing area for small contributing  
53 areas and increasing more slowly at larger contributing areas (i.e. the curve “flattens”).

54 Traditional FECs also have the potential problem that the maximum flood  
55 associated with smaller drainage basins may be biased upward (or the floods of larger  
56 drainage basins biased downward) because there are typically many more records of  
57 floods in smaller drainage basins relative to larger drainage basins (because there are  
58 necessarily fewer large drainage basins in any hydroclimatic region). That is, the largest  
59 flood of record for small drainage basins within a hydroclimatic region likely corresponds  
60 to a flood of a larger recurrence interval compared with the largest flood of record for  
61 larger drainage basins. In this paper we present a method that includes recurrence-interval

62 information and avoids any sample-size bias that might exist as a function of contributing  
63 area.

64 The use of FECs to quantify flood regimes is limited by the lack of recurrence-  
65 interval information (Wolman and Costa, 1984; Castellarin et al., 2005) and by the short  
66 length, incomplete nature, and sparseness of many flood-discharge records. Without  
67 recurrence-interval information, the data provided by FECs are difficult to apply to some  
68 research and planning questions related to floods. In the U.S. for example, the 100- and  
69 500-year flood events are the standard event sizes that define flood risk for land planning  
70 and engineering applications (FEMA, 2001).

71 Previously published studies have looked at new approaches to approve upon the  
72 FEC method. Castellarin et al. (2005) took a probabilistic approach to estimating the  
73 exceedance probability of the FEC for synthetic flood data. The authors were able to  
74 relate the FECs of certain recurrence intervals to the correlation between sites, the  
75 number of flood observations, and the length of each observation. Later, Castellarin  
76 (2007) and Castellarin et al. (2009) applied these methods to real flood record data and  
77 extreme rainfall events for basins within north-central Italy. Castellarin et al. (2009) also  
78 created depth-duration envelope curves of precipitation to relate extreme precipitation  
79 events to mean annual precipitation. This group of studies was successful in  
80 incorporating recurrence-interval information into the traditional FEC method. However,  
81 most of the models presented in these studies were completed with synthetic data or  
82 created for design storm processes and require additional analysis. Also, most of the  
83 precipitation data used in these past studies was collected using rain gauges (point  
84 sources), while only a small subset of data in Castellarin et al. (2009) was sourced from  
85 radar-derived precipitation estimates. In contrast to these studies we formulate a  
86 simplified method (i.e. the FMAC method) that is readily applicable to any region of  
87 interest and can be directly compared to already existing FECs. Also we favor the use of  
88 spatially complete radar-derived precipitation estimates in order to apply our methods to  
89 ungauged basins.

90 In this study, a new method for estimating flood discharges associated with user-  
91 specified recurrence intervals is introduced that uses radar-derived precipitation estimates  
92 (in this case rainfall only), combined with the diffusion-wave flow-routing algorithm, to

93 create frequency-magnitude-area curves (FMACs) of flood discharge. Our method (i.e.  
94 the FMAC method) retains the power of the FEC approach in that data from different  
95 drainage basins within a hydroclimatic region are aggregated by contributing area,  
96 thereby enabling large sample sizes to be obtained within each contributing-area class in  
97 order to more accurately constrain the frequencies of past extreme flood events and hence  
98 the probabilities of future extreme flood events within each class. The method improves  
99 upon the FEC approach in that the complete spatial coverage of radar-derived  
100 precipitation estimates provides for large sample sizes of most classes of contributing  
101 area (larger contributing areas have fewer samples). The radar-derived precipitation  
102 estimates include only rainfall and therefore snow and other types of precipitation are not  
103 included in the study. The precipitation estimates are then used to predict flood  
104 discharges associated with specific recurrence intervals by first accounting for water lost  
105 to infiltration and evapotranspiration using runoff coefficients appropriate for different  
106 contributing areas and antecedent-moisture conditions, and then routing the available  
107 water using a flow-routing algorithm. Predicted flood discharges are presented as FMACs  
108 on log-log plots, similar to traditional FECs, except that the method predicts a family of  
109 curves, one for each user-defined recurrence interval. These plots are then compared to  
110 FECs for the study region (Enzel et al., 1993) and the U.S. (Costa, 1987).

## 112 **1.2 Study Area**

113 This study focuses on the Upper and Lower Colorado River Basins (UCRB and  
114 LCRB, respectively; Fig. 1) as example applications of the FMAC method. Although the  
115 methods we develop are applied to the UCRB and LCRB in the western U.S. in this  
116 study, the methods are applicable to any region of interest where radar-derived  
117 precipitation estimates are available (i.e. the entire U.S. and at least 22 countries around  
118 the world; Li, 2013; RadarEU, 2014). We focus on the UCRB and LCRB because they  
119 have been a focus of flood-hazard assessment studies in the western U.S. and hence the  
120 FECs available for them are of especially high quality. In addition, the distinctly different  
121 hydroclimatic regions of the UCRB and LCRB (Sankarasubramanian and Vogel, 2003)  
122 make working in these regions an excellent opportunity to test and develop the new  
123 methods of this study on different precipitation patterns and storm types.



124           Precipitation and flooding in the LCRB are caused by convective-type storms,  
125 including those generated by the North American Monsoon (NAM), and frontal-type and  
126 tropical storms sourced from the Pacific Ocean and the Gulf of California (House and  
127 Hirschboeck, 1997; Etheredge et al., 2004). In the UCRB, the influence of the NAM and  
128 tropical storms is diminished and floods are generally caused by Pacific frontal-type  
129 storms (Hidalgo and Dracup, 2003). In both regions, the El Niño Southern Oscillation  
130 (ENSO) alters the frequency and intensity of the NAM, tropical storms, and the Pacific  
131 frontal systems, and can cause annual variations in precipitation and flooding (House and  
132 Hirschboeck, 1997; Hidalgo and Dracup, 2003). Winter storms in both regions are also  
133 intensified by the occurrence of atmospheric rivers (Dettinger et al., 2011), which can  
134 cause total winter precipitation to increase up to approximately 25% (Rutz and  
135 Steenburgh, 2012). The radar-derived precipitation estimates used in this study record  
136 this natural variability in precipitation in the two regions.

137           The methods used in this study to calculate precipitation and flood discharges of  
138 specified recurrence intervals from radar-derived precipitation estimates require a few  
139 main assumptions. The first assumption is that of climate stationarity, i.e. the parameters  
140 that define the distribution of floods do not change through time (Milly et al., 2008).  
141 Climate is changing and these changes pose a challenge to hazard predictions based on  
142 the frequencies of past events. Nevertheless, stationarity is a necessary assumption for  
143 any probabilistic analysis that uses past data to make future predictions. The results of  
144 such analyses provide useful starting points for more comprehensive analyses that  
145 include the effects of future climate changes. The second assumption is that the sample  
146 time interval is long enough to correctly represent the current hydroclimatic state (and its  
147 associated precipitation patterns and flood magnitudes and risks) of the specified study  
148 area. Our study uses data for the 1996 to 2004 water years and therefore may be limited  
149 by inadequate sampling of some types of rare weather patterns and climate fluctuations  
150 within that time interval. To address whether or not the sample time interval used in this  
151 study includes major changes in circulation and weather patterns, and therefore is a good  
152 representation of climate in the CRB, we investigated the effect of the El Niño Southern  
153 Oscillation (ENSO) on precipitation intensity within the UCRB and LCRB. ENSO is a  
154 well-known important influence on the hydroclimatology of the western U.S. (Hidalgo

155 and Dracup, 2003; Cañon et al., 2007). In general, winter precipitation in the  
156 southwestern U.S. increases during El Niño events and decreases during La Niña events  
157 (Hidalgo and Dracup, 2003). The opposite effects are found in the northwestern portions  
158 of the U.S. (including the UCRB; Hidalgo and Dracup, 2003). The last assumption of the  
159 method is that all basins of similar contributing area respond similarly to input  
160 precipitation, i.e. that they have similar flood-generating and flow-routing mechanisms.  
161 Specifically, the method assumes that basins of similar contributing area have the same  
162 runoff coefficient, flow-routing parameters, basin shape, and channel length, width, and  
163 slope. This assumption is necessary in order to aggregate data into discrete contributing-  
164 area classes so that the frequency of extreme events can be estimated from relatively  
165 short-duration records. In this study, high-recurrence-interval events (i.e. low frequency  
166 events) can be considered despite the relatively short length of radar-derived-  
167 precipitation-estimate records because the number of samples in the radar-derived record  
168 is extremely large, especially for small contributing areas and small duration floods. For  
169 example, for a 1-h time-interval-of-measurement and a contributing area of 4,096 km<sup>2</sup>  
170 event in the UCRB, there are approximately 40 (number of spatial scale samples) times  
171 55000 (number of temporal scale samples in nine years of data) samples of precipitation  
172 values (and associated modeled discharges obtained via flow routing). As contributing  
173 area and time intervals of measurement increase there are successively fewer samples,  
174 within any particular hydroclimatic region, thus increasing the uncertainty of the resulting  
175 probability assessment for larger areas and longer time periods.

176

## 177 **2. Next-Generation-Radar (NEXRAD) Data**

178 The specific radar-derived precipitation estimates we use in this study come from  
179 the Stage III Next-Generation-Radar (NEXRAD) gridded product, which is provided for  
180 the entire U.S., Guam, and Puerto Rico. NEXRAD was introduced in 1988 with the  
181 introduction of the Weather Surveillance Radar 1988 Doppler, or WSR-88D, network  
182 (Fulton et al., 1998). The WSR-88D radars use the Precipitation Processing System  
183 (PPS), a set of automated algorithms, to produce precipitation intensity estimates from  
184 reflectivity data. Reflectivity values are transformed to precipitation intensities through  
185 the empirical *Z-R* power-law relationship,

186  $Z = \alpha R^\beta$  (1)

187 where  $Z$  is precipitation rate ( $\text{mm h}^{-1}$ ),  $\alpha$  and  $\beta$  are derived empirically and can vary  
188 depending on location, season, and other conditions (Smith and Krajewski, 1993), and  $R$   
189 is reflectivity ( $\text{mm}^6 \text{m}^{-3}$ ; Smith and Krajewski, 1993; Fulton et al., 1998; Johnson et al.,  
190 1999). Precipitation intensity data are filtered and processed further to create the most  
191 complete and correct product (Smith and Krajewski, 1993; Smith et al., 1996; Fulton et  
192 al., 1998; Baek and Smith, 1998). Further information and details about PPS processing  
193 are thoroughly described by Fulton et al. (1998).

194 Stage III NEXRAD gridded products are Stage II precipitation products mapped  
195 onto the Hydrologic Rainfall Analysis Project (HRAP) grid (Shedd and Fulton, 1993).  
196 Stage II data are hourly precipitation intensity products that incorporate both radar  
197 reflectivity and rain-gauge data (Shedd and Fulton, 1993) in an attempt to make the most  
198 accurate precipitation estimates possible. The HRAP grid is a polar coordinate grid that  
199 covers the conterminous U.S., with an average grid size is 4 km by 4 km, although grid  
200 size varies from approximately 3.7 km (north to south) to 4.4 km (east to west) in the  
201 southern and northern U.S., respectively (Fulton et al., 1998).

202

### 203 **3. Methods**

#### 204 **3.1 NEXRAD Data Conversion and Sampling**

205 NEXRAD Stage III gridded products (hereafter NEXRAD products) for an area  
206 covering the Colorado River basin from 1996 to 2005 were downloaded from the NOAA  
207 HDSG website ([http://dipper.nws.noaa.gov/hdsb/data/nexrad/cbrfc\\_stageiii.php](http://dipper.nws.noaa.gov/hdsb/data/nexrad/cbrfc_stageiii.php)) for  
208 analysis. The data files were converted from archived XMRG files to ASCII format (each  
209 data file representing the mean precipitation intensity within each 1 h interval) using the  
210 `xmrctoasc.c` program provided on the NOAA HDSG website. The ASCII data files were  
211 then input into a custom program written in IDL for analysis.

212 We quantified hourly precipitation intensities ( $\text{mm h}^{-1}$ ) over square idealized  
213 basins (i.e. not real basins, but square basins as shown schematically in Fig. 2) of a range  
214 of areas from  $16 \text{ km}^2$  to  $11,664 \text{ km}^2$  (approximately the contributing area of the Bill  
215 Williams River, AZ, for readers familiar with the geography of the western U.S.) by  
216 successively spatially averaging precipitation-intensity values at HRAP pixel-length

217 scales of powers of two (e.g. 4, 16 pixel<sup>2</sup>, etc.) and three (e.g. 9, 81 pixel<sup>2</sup>, etc.; Fig. 2).  
218 Spatial averaging is done by both powers of 2 and 3 simply to include more points on the  
219 FMACs than would result from using powers of 2 or 3 alone. The number of samples  
220 within each contributing area class limited the range of contributing areas used in this  
221 study.

222 UCRB and LCRB boundaries from GIS hydrologic unit layers created by the  
223 USGS and provided online through the National Atlas site  
224 (<http://www.nationalatlas.gov/atlasftp.html#hucs00m>) were projected to HRAP  
225 coordinates using the methods of Reed and Maidment (2006). These boundaries were  
226 used to delineate the region from which precipitation data were sampled from the  
227 NEXRAD products, i.e. when averaging precipitation data by powers of two and three a  
228 candidate square drainage basin was not included in the analysis if any portion of the  
229 square fell outside of the boundaries of the UCRB or LCRB (Fig. 2). Throughout the  
230 analysis, the HRAP pixel size was approximated by a constant 4 km by 4 km size despite  
231 the fact that HRAP pixel sizes vary slightly as a function of latitude (Reed and Maidment,  
232 2006). Our study basins span latitudes between approximately 31°N and 43°N resulting  
233 in a maximum error of 15%. However, by keeping the pixel size constant, all pixels could  
234 be treated as identical in size and shape allowing us to sample the NEXRAD products in  
235 an efficient and automated way over many spatial scales.

236 For larger contributing areas, necessarily fewer samples are available within a  
237 given hydroclimatic region, thus increasing the uncertainty associated with the analysis  
238 for those larger contributing-area classes. For the UCRB and LCRB specifically, the  
239 uncertainty in the analysis becomes significant for contributing-area classes equal to and  
240 larger than  $\sim 10^3$  to  $10^4$  km<sup>2</sup> depending on the recurrence interval being analyzed. Of  
241 course, if the hydroclimatic region is defined to be larger, more samples are available for  
242 each contributing-area class and hence larger basins can be analyzed with confidence.

243 In addition to computing precipitation intensities as a function of spatial scale, we  
244 averaged precipitation intensities as a function of the time interval of measurement  
245 ranging from 1 to 64 hours in powers of two by averaging contiguous hourly precipitation  
246 intensity records over the entire 9-year study period. This range in time intervals was

247 chosen in order to capture precipitation events that last on the order of ~1 hour  
248 (convective-type storms) to days (frontal-type storms).

249

### 250 **3.2 Precipitation and Flood Calculations**

251 Two types of variables were calculated from the precipitation intensities sampled  
252 over the contributing-area and time-interval-of-measurement classes: (1) precipitation  
253 discharge,  $Q_p$ , and (2) peak flood discharge,  $Q_{fd}$ . The variable  $Q_p$  is defined as the  
254 average precipitation intensity over a basin and time interval of measurement multiplied  
255 by the contributing area, resulting in units of  $m^3 s^{-1}$ . The variable  $Q_{fd}$  is the peak flood  
256 discharge ( $m^3 s^{-1}$ ) calculated via the diffusion-wave flow-routing algorithm for a  
257 hypothetical flood triggered by a precipitation discharge,  $Q_p$ , input uniformly over the  
258 time interval of measurement to idealized square basins associated with each  
259 contributing-area class.

260 The flow-routing algorithm we employ does not explicitly include infiltration and  
261 other losses that can further reduce  $Q_{fd}$  relative to  $Q_p$ . In this study we modeled  
262 infiltration and evaporation losses by simply removing a volume of water per unit time  
263 equal to one minus the runoff coefficient, i.e. the ratio of runoff to precipitation over a  
264 specified time interval, for three antecedent-moisture scenarios (wet, med, and dry). We  
265 estimated runoff coefficients for each contributing-area class and each of three  
266 antecedent-moisture scenarios using published values for annual runoff coefficients for  
267 large basins within the UCRB and LCRB (Rosenburg et al., 2013) and published values  
268 for event-based runoff coefficients for small basins modeled with a range of antecedent-  
269 moisture conditions by Vivoni et al. (2007) (Fig. 3). On average, estimated runoff  
270 coefficients are higher for smaller and/or initially wetter basins. We found the  
271 dependence of runoff coefficients on contributing area and antecedent moisture to be  
272 similar despite the large difference in time scales between event-based and annual values.  
273 Despite the difference in geographic region between our study site and that of Vivoni et  
274 al. (2007) (they studied basins in Oklahoma), the runoff coefficients they estimated are  
275 likely to be broadly applicable to the LCRB and UCRB given that basin size and  
276 antecedent moisture are the primary controls on these values (climate and soil types play  
277 a lesser role except for extreme cases).

278 We applied the estimated runoff coefficients for all three antecedent-moisture  
279 scenarios by simply using them to remove a portion of the  $Q_p$  calculated for specific time  
280 interval and basin area

$$282 \quad Q_{pm} = C * Q_p \quad (2)$$

283  
284 where  $C$  is the runoff coefficient calculated for the specific basin area and antecedent-  
285 moisture scenario under evaluation. The newly formed  $Q_{pm}$  is now the  $Q_p$  value for the  
286 wet, medium, or dry antecedent-moisture scenario under analysis.

287 The flow-routing algorithm routes flow along the main-stem channel of idealized  
288 square basins with sizes equal to the contributing area of each contributing-area class.  
289 The choice of a square basin is consistent with the square sample areas (see Section 3.1)  
290 and it allows for basin shape to remain the same (and therefore comparable) over the  
291 range of contributing areas used in this study. The main-stem channel, with a length of  $L$   
292 (m), was defined as the diagonal distance from one corner to the opposite corner across  
293 the square basin (i.e.  $L$  is equal to the square root of two times the area of the square  
294 basin). This main-stem channel was used in conjunction with a normalized area function  
295 to represent the shape of the basin and the routing of runoff through the drainage basin  
296 network. By including the normalized area function, we can account for geomorphic  
297 dispersion (i.e. the attenuation of the flood peak due to the fact that precipitation that falls  
298 on the landscape will take different paths to the outlet and hence reach the outlet at  
299 different times) in our analyses. The normalized area function,  $A(x)$  (unitless), is defined  
300 as the portion of basin area,  $A_T(x)$  ( $m^2$ ), that contributes flow to the main-stem channel  
301 within a given range of distances ( $x$ ) from the outlet, normalized by the total basin area,  
302  $A_T$  ( $m^2$ ; Mesa and Mifflin, 1986; Moussa, 2008). The normalized area function is  
303 assumed to be triangular in shape with a maximum value at the midpoint of the main-  
304 stem channel from the outlet. Area functions, and related width functions, from real  
305 basins used in other studies show this triangular shape in general (Marani et al., 1994;  
306 Rinaldo et al., 1995; Veneziano et al., 2000; Rodriguez-Iturbe and Rinaldo, 2001; Puente  
307 and Sivakumar, 2003; Saco and Kumar, 2008), although not all basins show this shape.  
308 The triangular area function has been shown to approximate the average area function of

309 basins and that the peak discharge and time to peak discharge is likely more important to  
310 the shape of the flood wave (Henderson, 1963; Rodriguez-Iturbe and Valdes, 1979).

311 A 1-dimensional channel with simplified width and along-channel slope  
312 appropriate for channels in the CRB is used to approximate the geometry of the main-  
313 stem channel of the idealized basin in the flow-routing algorithm. In addition, values for  
314 channel slope,  $S$  (m/m), and channel width,  $w$  (m), are assigned based on the contributing  
315 area of the idealized basin and the results of a least-squares regression to channel-slope  
316 and channel-width data from the CRB. We assume here that the assigned channel slopes  
317 and widths represent the average value for the entire idealized basin. To find the best  
318 approximations for channel slope and width values, we developed formulae that predict  
319 average channel slope and channel width as a function of contributing area based on a  
320 least-squares fit of the logarithms of slope, width, and contributing area based on  
321 approximately 100 sites in the Colorado River Basin (CRB; Fig. 4). The data used in  
322 these least-squares regressions included slope, width, and contributing area information  
323 from all sites in the LCRB and southern UCRB presented in Moody et al. (2003) and  
324 additional sites from USGS stream-gauge sites from across the CRB.

325 The assigned channel slope and width values, together with the values of  $Q_{pm}$   
326 modified for each antecedent-moisture scenario, were used to calculate the depth-average  
327 velocities,  $V$  ( $m\ s^{-1}$ ), in hypothetical 1D main-stem channels of idealized square drainage  
328 basins corresponding to each contributing-area and time-interval-of-measurement class.  
329 In this study, flow velocity is not modeled over space and time, but rather is set at a  
330 constant value appropriate for the peak discharge using an iterative approach that solves  
331 for the peak depth-averaged flow velocity, uses that velocity to compute the parameters  
332 of the diffusion-wave-routing algorithm, routes the flow, and then computes an updated  
333 estimate of peak depth-averaged velocity. To calculate the depth-averaged velocity,  $V$ , we  
334 used Manning's equation, i.e.

$$335 \quad V = \frac{1}{n_M} R^{\frac{2}{3}} S^{\frac{1}{2}}, \quad (3)$$

336 where  $n_M$  is Manning's  $n$  (assumed to be equal to 0.035), and  $R$  is the hydraulic radius  
337 (m) calculated with the assigned channel width, and  $S$  (m/m) is the assigned channel  
338 slope. In order to calculate  $R$ , water depth,  $h$ , of the peak discharge needed to be

339 determined. In this study  $h$  was iteratively solved for based on the peak-flow conditions  
 340 (i.e. the depth-averaged velocity,  $V$ , associated with the peak-flood discharge,  $Q_{fd}$ ) with  $h$   
 341 set at 1 m for the first calculation of the flow-routing algorithm. At the end of each  
 342 calculation,  $h$  is recalculated using Manning's equation. These iterations continue until  
 343 the water depth converges on a value (i.e. the change from the last calculation of  $h$  to the  
 344 next calculation of  $h$  is  $\leq 0.1$  m) corresponding to a specific recurrence interval,  
 345 contributing-area class, and time-interval-of-measurement class.

346 The method we used to model flow through the main-stem channel is the  
 347 diffusion-wave flow-routing algorithm. This approach is based on the linearized Saint-  
 348 Venant equations for shallow-water flow in one dimension. To find a simpler, linear  
 349 solution to Saint-Venant equations, Brutsaert (1973) removed the acceleration term from  
 350 the equations, leaving the diffusion and advection terms that often provide a reasonable  
 351 approximation for watershed runoff modeling (Brutsaert, 1973). Leaving the diffusion  
 352 term in the flow-routing algorithm includes hydrodynamic dispersion of the flood wave  
 353 in the calculation of the flood hydrograph. In the case where the initial condition is given  
 354 by a unit impulse function (Dirac function), the cell response function of the channel,  $q_d$   
 355 (units of  $s^{-1}$ ), is given by:

$$356 \left| q_d = \frac{x}{(2\pi)^{1/2} b t_r^{3/2}} \exp\left[-\frac{(x - a t_r)^2}{2 b^2 t_r}\right] \right. \quad (4)$$

357 where  $x$  is the distance along the channel from the location where the impulse is input to  
 358 the channel,  $t_r$  is time since the impulse was input into the channel, and the drift velocity  
 359  $a$  ( $m s^{-1}$ ) and diffusion coefficient  $b^2$  ( $m^2 s^{-1}$ ) are defined as

$$360 \left| a = (1 + a_0)V \right. \quad (5)$$

$$361 \left| b^2 = \frac{V^3}{g S F^2} (1 - a_0^2 F^2) \right. \quad (6)$$

362 where  $F$  is the Froude number,  $g$  is the acceleration due to gravity ( $m s^{-2}$ ), and  $a_0$  is a  
 363 constant equal to 2/3 when using Manning's equation (Troch et al., 1994). The large  
 364 floods modeled in this study are assumed to have critical-flow conditions and therefore  
 365 the Froude number is set to a constant value of 1.

366 The unit response discharge,  $q_{fd}$  ( $m^2 s^{-1}$ ), at the outlet of a drainage basin can be  
 367 computed from equations (3)-(5) by integrating the product of the cell response function



368  $q_d(x,t)$  corresponding to a delta-function input of the normalized area function,  $A(x)$ , i.e.  
369 the spatial distribution of precipitation input. The integral is given by

$$370 \left| q_{fd}(t_r) = \int_0^{t_p} \frac{Q_p}{w} dt' \int_0^L q_d(x, t_r - t') A(x) dx \right. \quad (7)$$

371 where  $t_p$  is the time interval of measurement over which the unit impulse input (i.e.  $Q_p$ ) is  
372 applied to the idealized square drainage basin, and  $t_r$  is the time after the input of the unit  
373 impulse that is long enough to capture the waxing the waning portions and the flood peak  
374 of the flood wave. The final peak discharge value, or  $Q_{fd}$  ( $m^3 s^{-1}$ ), was calculated by  
375 multiplying the unit discharge  $q_{fd}$  ( $m^2 s^{-1}$ ) by the channel width found through the formula  
376 derived from CRB data in Figure 4, and then selecting the largest value from the resulting  
377 hydrograph.

378

### 379 3.3 Recurrence Interval Calculations

380 To determine the precipitation-intensity values and  $Q_p$ , associated with a user-  
381 specified recurrence interval, maximum precipitation intensities of storm events sampled  
382 from the NEXRAD data for each contributing-area and time-interval-of-measurement  
383 class was first ranked from highest to lowest. Storm events were identified as adjacent  
384 precipitation intensity values separated by instances of zero values in time for each  
385 spatial scale. The relationship between recurrence intervals and rank in the ordered list is  
386 given by the probability-of-exceedance equation:

$$387 \left| RI = \frac{(n + 1)}{m} \right. \quad (8)$$

388 where  $RI$  is the recurrence interval (yr), defined as the inverse of frequency ( $yr^{-1}$ ) or  
389 probability of exceedance,  $n$  is the total number of samples in each contributing-area and  
390 time-interval-of-measurement scaled to units in years (resulting in units of yr), and  $m$  is  
391 the rank of the magnitude ordered from largest to smallest (unitless). The resulting  
392 precipitation intensities associated with a user-specified recurrence interval and  
393 contributing-area and time-interval-of-measurement class was then used to calculate the  
394  $Q_p$  value.

395 At the end of the calculations described above we have datasets of precipitation-  
396 intensity,  $Q_p$ , and  $Q_{fd}$  values for each combination of the eight contributing-area classes,

397 the seven time-interval-of-measurement classes, and the four recurrence intervals. We  
398 then find the maximum values of precipitation intensity,  $Q_p$ , and  $Q_{fd}$  associated with a  
399 given contributing-area class and recurrence interval among all values of the time-  
400 interval-of-measurement class (i.e. the values calculated for 1 to 64 h time intervals). This  
401 step is necessary in order to find the maximum values for a given contributing area class  
402 and recurrence interval independent of the time-interval-of-measurement, i.e.  
403 independent of storm durations and associated types of storms. These maximum values  
404 are used to plot the FMAC for a given recurrence interval.

405

### 406 **3.4 Estimation of Uncertainty**

407 Confidence intervals (i.e. uncertainty estimates) were calculated to quantify the  
408 uncertainty in calculated precipitation intensities and associated  $Q_p$  and  $Q_{fd}$  values. In this  
409 study we estimated confidence intervals using a non-parametric method similar to that  
410 used to calculate quantiles for flow-duration curves (Parzen, 1979; Vogel and Fennessey,  
411 1994). Like quantile calculations, which identify a subset of the ranked data in the  
412 vicinity of each data point to estimate expected values and associated uncertainties, we  
413 estimated confidence intervals for our predictions based on the difference in  $Q_p$  values  
414 between each point and the next largest value in the ranked list. This approach quantifies  
415 the variation in the precipitation intensity value for a given contributing area and  
416 recurrence interval. In some cases the calculated uncertainties for precipitation intensities  
417 and associated  $Q_p$  and  $Q_{fd}$  values are infinite due to the values being past the frequency-  
418 magnitude distribution, i.e. there are not enough samples for these values to be  
419 determined and there are no finite numbers to sample. These values are not used in this  
420 study.

421 The resulting confidence intervals of precipitation intensity were used to calculate  
422 confidence intervals for  $Q_p$  and  $Q_{fd}$ . Confidence intervals for  $Q_p$  values were equal to the  
423 confidence intervals for precipitation intensity propagated through the calculation of  $Q_p$   
424 (i.e. multiplying by contributing area). Confidence intervals for  $Q_{fd}$  values were  
425 calculated to be the same proportion of the  $Q_{fd}$  value as that set by the precipitation  
426 intensity value and its confidence intervals. For example, if the upper confidence interval  
427 was 120% of a precipitation intensity value, the upper confidence interval for the  $Q_{fd}$

428 value associated with the precipitation intensity value is assumed to be 120% of the  $Q_{fd}$   
429 value. This approach to propagation of uncertainty treats all other variables in the  
430 calculations as constants and additional uncertainty related to regression analyses on  
431 variables used in the flow-routing algorithm such as slope, channel width, and runoff  
432 coefficients was not included.

433

### 434 **3.5 Testing the Effects of Climate Variability**

435 To quantify the robustness of our results with respect to climate variability, we  
436 separated the NEXRAD data into El Niño and La Niña months using the multivariate  
437 ENSO index (MEI). All months of data with negative MEI values (La Niña conditions)  
438 were run together to calculate the precipitation intensity and  $Q_p$  values for contributing  
439 areas of 16, 256, and 4096 km<sup>2</sup>, time intervals of 1 to 64 hours, and for 10-, 50-, 100-,  
440 and 500-year recurrence intervals. This was repeated with all months of data with  
441 positive MEI values (El Niño conditions). Figure 5 shows the distribution of negative and  
442 positive MEI values during the 1996 to 2004 water years used in this study.

443

## 444 **4. Results**

### 445 **4.1 Channel Characteristics and Runoff Coefficients**

446 Least-squares regression of channel slopes and channel widths from the CRB  
447 versus contributing area was used to estimate channel slope, channel width, and runoff  
448 coefficients for each idealized basin of a specific contributing-area class. Channel slope  
449 decreases as a power-law function of contributing area with an exponent of -0.30 ( $R^2 =$   
450 0.39), whereas channel width increases as a power-law function of contributing area with  
451 an exponent of 0.28 ( $R^2 = 0.65$ ; Fig. 4). These results follow the expected relationships  
452 among channel slopes, widths, and contributing area, i.e. as contributing area increases  
453 the channel slope decreases and the channel width increases.

454 Runoff coefficients for wet, medium, and dry antecedent-moisture conditions all  
455 decrease with increasing contributing area following a logarithmic function, with the  
456 slope of the line decreasing from wet to dry conditions. The fitness of the line to the data  
457 also decreases for the wet to dry conditions, with the  $R^2$  values for wet, medium, and dry  
458 conditions equal to 0.78, 0.45, and 0.04, respectively. Runoff coefficients decrease with

459 increasing contributing area due to the increased probability of water losses as basin area  
460 increases. Also, as expected, runoff coefficients are highest in basins with wet initial  
461 conditions that are primed to limit infiltration and evapotranspiration.

462

## 463 **4.2 Trends in Precipitation Intensity**

464 Maximum precipitation intensities (i.e. the maximum among all time-interval-of-  
465 measurement classes) for each contributing-area class and recurrence interval decrease  
466 systematically as power-law functions of increasing contributing area for all recurrence  
467 intervals with an average exponent of  $-0.18 \pm 0.06$  (error is the standard deviation of all  
468 calculated exponents found from a weighed least-squares regression; average coefficient  
469 of determination  $R^2 = 0.78$ ). Note that maximum-precipitation-intensity results are not  
470 presented because they are closely related to the plots of  $Q_p$  versus contributing area in  
471 Figure 6, i.e.  $Q_p$  is simply the precipitation intensity multiplied by the contributing area.  
472 The decrease in maximum precipitation intensity with contributing area can be seen in  
473 Table 1, where maximum precipitation intensities over contributing areas of 11,664 km<sup>2</sup>  
474 are 45% to 8% of maximum precipitation intensity values for basin areas of 16 km<sup>2</sup> in  
475 both the UCRB and LCRB (Table 1). The largest decrease in maximum precipitation  
476 intensity values between the smallest and largest contributing areas were found for the  
477 largest recurrence interval (e.g. 500-year) for both the UCRB and LCRB. The decrease in  
478 maximum precipitation intensity with increasing contributing area suggests that there is a  
479 spatial limitation to storms of a given precipitation intensity.

480 Differences among maximum precipitation intensities for the four recurrence  
481 intervals as a function of contributing area are larger in the UCRB than in the LCRB  
482 (Table 1). This larger “spread” in the maximum precipitation intensities in the UCRB  
483 relative to the LCRB is also propagated throughout the maximum precipitation and flood  
484 discharge calculations. For both the UCRB and LCRB, the difference between the 50-  
485 and 100-year recurrence interval values was the smallest (Table 1). These trends show  
486 that maximum precipitation intensities vary much more as a function of recurrence  
487 interval in the UCRB compared with the LCRB.

488 Maximum precipitation intensities associated with a 10-year recurrence interval  
489 are similar in the LCRB and UCRB, while intensities were higher in the UCRB than the

490 LCRB for recurrence intervals of 50-, 100-, and 500-years (Table 1). The results of the  
491 comparison between the two basins suggest that common (i.e. low-recurrence-interval)  
492 precipitation events will have similar maximum precipitation intensities in the UCRB and  
493 LCRB, but that rare (i.e. high-recurrence-interval) precipitation events will have higher  
494 maximum precipitation intensities in the UCRB than in the LCRB for the same  
495 recurrence interval.

496

### 497 4.3 Trends in $Q_p$

498 Maximum precipitation discharges ( $Q_p$  hereafter) increase with contributing area  
499 as power-law functions with an average exponent of  $0.82 \pm 0.06$  (error is the standard  
500 deviation of all calculated exponents) based on weighed least-squares regressions on the  
501 data ( $R^2 = 0.98$ ) for all recurrence intervals and for both the UCRB and LCRB (Fig. 6).  
502 These  $Q_p$  values for a given contributing-area class and recurrence interval are the largest  
503 values taken from the multiple values calculated for each of the seven time intervals of  
504 measurement as explained in Section 3.3. By taking the maximum values, the resulting  
505  $Q_p$  FMACs approximate the upper envelope of values of a given recurrence interval. In  
506 this study the FMAC follows a power-law function that shows that  $Q_p$  increases  
507 predictably across the range in contributing areas. As with the maximum precipitation  
508 intensity results, differences between  $Q_p$  values of different recurrence intervals for a  
509 given contributing area were larger for the UCRB than the LCRB (Fig. 6).

510 In general, confidence intervals for  $Q_p$  values increase with increasing  
511 contributing-area class (Table 1 and Fig. 6). The large values of the highest contributing-  
512 area classes and highest recurrence intervals show the spatial limitation of the method,  
513 meaning that at these contributing-area classes and recurrence intervals the values are  
514 sampled from the largest ranked value and have infinite confidence intervals. These  
515 values include the 50-, 100-, and 500-year recurrence intervals for the UCRB and the  
516 100- and 500-year recurrence intervals for the LCRB at the 11,664 km<sup>2</sup> contributing-area  
517 class. These values also include the 100- and 500-year recurrence intervals for the UCRB  
518 and the 500-year recurrence intervals for the LCRB at the 4,096 km<sup>2</sup> contributing-area  
519 class. Values with infinite confidence intervals are not included in Fig. 6 due to their high  
520 uncertainties.

521

#### 522 4.4 Trends in $Q_{fd}$

523 Maximum  $Q_{fd}$  values (hereafter  $Q_{fd}$ ), i.e. the largest values taken for the multiple  
524 values calculated for each time interval of measurement for a given contributing-area  
525 class and recurrence interval, were used to plot FMACs for wet, medium, and dry  
526 conditions for both the UCRB and LCRB (Fig. 7). In general, FMACs for  $Q_{fd}$  values  
527 follow the power-law relationship shown in the  $Q_p$  FMACs until contributing areas of  
528  $\sim 1,000 \text{ km}^2$ , where the curves begin to very slightly flatten or decrease. As with the  $Q_p$   
529 values,  $Q_{fd}$  values representing some of the higher recurrence intervals converge to the  
530 same value (i.e. the value corresponding to the highest precipitation intensity for the  
531 contributing-area class) at contributing areas of  $\approx 10,000 \text{ km}^2$  and the confidence  
532 intervals become infinite (Table 2). This convergence of  $Q_{fd}$  values at the largest  
533 contributing areas is due to the reduction in the range of values and the number of  
534 samples from which to calculate the associated values for each recurrence interval.

535 In general, The UCRB  $Q_{fd}$  FMACs (Fig. 7A, C, and E) are slightly higher in  
536 magnitude and span a larger range of magnitudes than the FMACs for the LCRB. For  
537 both basins, FMACs for the wet, medium, and dry conditions resulting in the highest,  
538 middle, and lowest magnitudes, respectively. This trend is expected due to the lowering  
539 of runoff coefficients and available water as conditions become drier.

540 FMACs of  $Q_{fd}$  for the LCRB plot below published FECs for the LCRB and U.S.  
541 (Fig. 7B, D, F) at low contributing areas, but meet and/or exceed the LCRB FEC for  
542 contributing areas above  $\approx 1,000 \text{ km}^2$  and  $\approx 100 \text{ km}^2$  for dry and wet antecedent-moisture  
543 conditions, respectively. The FMACs for the LCRB do not exceed the U.S. FEC. All of  
544 the FMACs of  $Q_{fd}$  for the UCRB exceed the LCRB FEC for wet conditions, with the  
545 FMACs of lower recurrence intervals exceeding the curve at higher contributing areas  
546 than the FMACs of higher recurrence intervals (Fig. 7A). The 500-year FMAC for wet  
547 conditions approximate the U.S. FEC for contributing areas between  $\approx 100$  to  $1,000 \text{ km}^2$ .  
548 These results suggests that under certain antecedent-moisture conditions, and in basins of  
549 certain contributing areas, the LCRB produces floods that exceed the maximum recorded  
550 floods in the LCRB and the UCRB produces floods of magnitudes on par with the  
551 maximum recorded floods in the U.S.

552

#### 553 **4.5 The Effects of ENSO on Precipitation**

554 Definitive differences in maximum precipitation intensities and  $Q_p$  values were  
555 found between months with positive versus months with negative MEI values (Table 3).  
556 For very small contributing areas (16 km<sup>2</sup>) in the LCRB maximum precipitation  
557 intensities and  $Q_p$  values are similar during negative and positive MEI conditions. Larger  
558 contributing areas (256 and 4,096 km<sup>2</sup>) show higher maximum precipitation intensities  
559 during negative MEI conditions regardless of recurrence interval. Values of  $Q_p$  show the  
560 same trend as the maximum precipitation intensity in the LCRB. In the UCRB, maximum  
561 precipitation intensities and  $Q_p$  values during negative MEI conditions are higher than  
562 those during positive MEI conditions regardless of recurrence interval.

563

### 564 **5. Discussion**

#### 565 **5.1 Use and Accuracy of NEXRAD Products**

566 NEXRAD products are widely used as precipitation inputs in rainfall-runoff  
567 modeling studies due to the spatially complete nature of the data necessary for hydrologic  
568 and atmospheric models (Ogden and Julien, 1994; Giannoni et al., 2003; Kang and  
569 Merwade, 2011). In contrast to past studies similar in scope to this study (Castellarin et  
570 al., 2005; Castellarin, 2007; Castellarin et al., 2009) we did not use rain-gauge data and  
571 only used NEXRAD products to determine the FMACs for precipitation and flood  
572 discharges. We favor NEXRAD products due to the spatial completeness of the data.

573 Intuitively, NEXRAD products that are spatially complete and that average  
574 precipitation over a 4 km by 4 km area would not be expected to match rain-gauge data  
575 within that area precisely (due to the multi-scale variability of rainfall), although some  
576 studies have tried to address this discrepancy (Sivapalan and Blöschl, 1998; Johnson et  
577 al., 1999). Xie et al. (2006) studied a semi-arid region in central New Mexico and found  
578 that hourly NEXRAD products overestimated the mean precipitation relative to rain-  
579 gauge data in both monsoon and non-monsoon seasons by upwards of 33% and 55%,  
580 respectively. Overestimation of precipitation has also been noted due to the range and the  
581 tilt angle at which radar reflectivity data are collected (Smith et al., 1996).

582 Underestimation of precipitation by NEXRAD products relative to rain gauge data has  
583 also been observed (Smith et al., 1996; Johnson et al., 1999), however.

584 Under- and over-estimation of precipitation by NEXRAD products in relation to  
585 rain-gauge data is partly due to the difference in sampling between areal NEXRAD  
586 products and point data from rain gauges and partly due to sampling errors inherent to  
587 both methods. For example, NEXRAD products include problems such as the use of  
588 incorrect Z-R relationships for high intensity storms and different types of precipitation,  
589 such as snow and hail (Baeck and Smith, 1998). Also, because of its low reflectivity,  
590 snow in the NEXRAD products is measured as if it were light rain (David Kitzmiller,  
591 personal communication, January 10, 2012). This means the NEXRAD products likely  
592 underestimate snowfall and therefore snowfall is not fully accounted for in this study.  
593 Due to snowfall not being included in this study, associated snowpack and snowmelt  
594 effects were also not accounted for. Rain gauges can also suffer from a number of  
595 measurement errors that usually result in an underestimation of rainfall (Burton and Pitt,  
596 2001). In addition, gridded rainfall data derived from rain gauges are not spatially  
597 complete and therefore must be interpolated between point measurements to form a  
598 spatially complete model of rainfall. It is impossible to discern which product is more  
599 correct due to the differences in measurement techniques and errors, but by taking both  
600 products and combining them into one, the Stage III NEXRAD precipitation products  
601 generate the best precipitation estimate possible for this study. Moreover, it should be  
602 noted that 100-year flood magnitude predictions based on regression equations have very  
603 large relative error bars (ranging between 37 to 120% in the western U.S.; Parrett and  
604 Johnson, 2003) and that measurements of past extreme floods can have significant errors  
605 ranging from 25% to 130% depending on the method used (Baker, 1987). As such, even a  
606 ~50% bias in NEXRAD-product-derived precipitation estimates is on par or smaller than  
607 the uncertainty associated with an analysis of extreme flood events.

608 As stated previously, the NEXRAD precipitation estimates used here do not  
609 include snowfall and other non-rainfall precipitation types. In this study we also do not  
610 include snowpack information into our flood discharge calculations. The omission of  
611 snowpack is a reasonable assumption for our low elevation, warm regions within most of  
612 the UCRB and LCRB. However, we acknowledge some of our higher elevation areas at



613 | higher latitudes may be underestimating the maximum flood discharge by only including  
614 | rainfall-derived runoff. If the methodology in this paper were applied to a snowmelt-  
615 | dominated region, snowpack would need to be added to accurately estimate the  
616 | maximum flood discharge.

## 618 | **5.2 Comparison of FMACs to Published FECs**

619 | FMACs of  $Q_{fd}$  exhibit a similar shape and similar overall range in magnitudes as  
620 | previously published FECs, derived from stream-gauge and paleoflood records, for the  
621 | LCRB and U.S. (Fig. 7). In general, the FMACs exceed or match published FECs at  
622 | larger contributing areas, and are lower than or on par with published FECs at the  
623 | smallest contributing areas (Fig. 7).

624 | All FMACs except the 500-year recurrence-interval curve for the UCRB under  
625 | wet conditions are positioned well below the U.S. FEC presented by Costa (1987; Fig.  
626 | 7A). The similarity between the 500-year recurrence interval  $Q_{fd}$  FMAC for the UCRB  
627 | under wet conditions and the U.S. FEC suggests that the U.S. FEC includes floods of  
628 | larger recurrence-intervals, which are similar in magnitude to the 500-year recurrence-  
629 | interval floods within the UCRB. The approximation of the U.S. FEC by the 500-year  
630 | UCRB FMAC is a significant finding due to the fact that the U.S. FEC includes storms  
631 | from other regions of the U.S. with extreme climatic forcings (i.e. hurricanes, extreme  
632 | convection storms, etc.).

633 | The  $Q_{fd}$  FMACs for the LCRB can be directly compared to the FEC for the LCRB  
634 | presented by Enzel et al. (1993). At contributing areas smaller than approximately 100  
635 | km<sup>2</sup>,  $Q_{fd}$  FMACs for wet conditions and all recurrence intervals are positioned below the  
636 | LCRB FEC, but at larger contributing areas  $Q_{fd}$  FMACs exceed or approximate the  
637 | LCRB FEC.  $Q_{fd}$  FMACs calculated for medium and dry antecedent conditions show the  
638 | same trend, but exceed the LCRB FEC at a larger contributing areas ( $\geq 1,000$  km<sup>2</sup>). This  
639 | comparison suggests that although the FMACs overlap the overall range of flood  
640 | magnitudes of the LCRB FEC, the two methods are not capturing the same trend for  
641 | extreme flood discharges and the LCRB is capable of producing floods larger than those  
642 | on record.

643           The difference in the slope of the FMACs, and specifically the exceedance of the  
644 published LCRB FEC, suggests that the two methods are not capturing the same  
645 information. This difference may be due to the difference in how the data are sourced for  
646 each method. FECs are created as regional estimates of maximum flood discharges and  
647 are based on stream-gauging station and paleoflood data. The FECs are then used to  
648 provide flood information for the region, including ungauged and unstudied drainage  
649 basins. FECs are limited to the number of stream gauges employed by public and private  
650 parties and do not include all basins within a region. In general, FECs may underestimate  
651 maximum floods in larger basins, relative to smaller basins, because there are a larger  
652 number of smaller basins to sample than larger basins. This sample-size problem  
653 introduces bias in the record where flood estimates for smaller contributing areas may be  
654 more correct than estimates for larger basins. In this study, the regional precipitation  
655 information given by the NEXRAD network is used to form the FMAC, therefore taking  
656 advantage of the entire region and using precipitation data to calculate flood discharges,  
657 rather than directly measuring flood discharges. This sampling scheme allows for much  
658 larger sample sizes for the range of contributing areas, therefore minimizing the sample  
659 bias of the traditional FEC.

660           This study aimed to introduce the new method of the FMAC and therefore  
661 improve upon the traditional methods of the FEC. By calculating FMACs we provide  
662 frequency and magnitude information of possible flood events for a given region in  
663 contrast to the FECs that only provide an estimate of the largest flood on record. This  
664 information is vital for planning and infrastructure decisions and the accurate  
665 representation of precipitation and flooding in design-storm and watershed modeling. In  
666 addition, the fact that the FMACs match the FECs for large (500-year) recurrence  
667 intervals and do not exhibit the same trends suggests that the FMACs are capturing  
668 different samples than the FECs. This indicates that by using the NEXRAD products, the  
669 FMACs may provide a more inclusive flood dataset for a region (especially ungauged  
670 areas) than the traditional stream-gauge records.

671

672 | **5.3 Precipitation Controls on the Form of the FEC**

673  $Q_p$  FMACs were shown to have a strong (average  $R^2 = 0.93$ ) power-law  
674 relationship between  $Q_p$  and contributing area for all recurrence intervals. Figure 8 shows  
675 a conceptualized FEC where the concave-down shape is created when the observed  
676 envelope curve diverges from the constant positive power-law relationship between  $Q_p$   
677 and contributing area. This diversion creates a “gap” between the two curves and  
678 indicates that flood discharge is not a simple power-law function of contributing area.  
679 Three mechanisms have been proposed to explain the “gap” and characteristic concave-  
680 down shape of FECs: (1) integrated precipitation (i.e. total precipitation over an area) is  
681 more limited over larger contributing areas compared to smaller contributing areas  
682 (Costa, 1987), (2) a relative decrease in maximum flood discharges in larger contributing  
683 areas due to geomorphic dispersion (Rodriguez-Iturbe and Valdes, 1979, Rinaldo et al.,  
684 1991, Saco and Kumar, 2004), and (3) a relative decrease in maximum flood discharges  
685 in larger basins due to hydrodynamic dispersion (Rinaldo et al., 1991). The first  
686 explanation, proposed by Costa (1987), suggests that there is a limitation to the size of a  
687 storm and the amount of water that a storm can precipitate. The effect of precipitation  
688 limitations may be evidenced by the decreasing maximum precipitation intensities with  
689 increasing contributing area. However, the strong power-law relationship between  $Q_p$  and  
690 contributing area for all recurrence intervals indicates that  $Q_p$  is, in general, increasing  
691 predictably over the range of contributing areas used in this study. Even if precipitation  
692 limitations affect the shape of the curve, this single hypothesis does not account for all of  
693 the concave-down shape of each FEC suggesting that other mechanisms are important to  
694 creating the characteristic shape. However, it is important to note that the importance of  
695 each mechanism may be different for different locations.

696

#### 697 | **5.4 Climate Variability in the NEXRAD Data**

698 The results from comparing negative and positive MEI conditions in the UCRB  
699 and LCRB are generally consistent with ideas about ENSO and how it affects  
700 precipitation in the western U.S. In the LCRB, during negative MEI conditions, small,  
701 frequent storms have similar or slightly higher maximum precipitation intensities and  $Q_p$   
702 values than during positive MEI conditions. This similarity between the two conditions  
703 may be explained by the balancing of increased winter moisture during El Niño in the

704 southwestern U.S. (Hidalgo and Dracup, 2003) and increased summer moisture through  
705 the strengthening of the NAM system and the convective storms it produces during La  
706 Niña conditions (Castro et al., 2001; Grantz et al., 2007). In general, the strengthening of  
707 the NAM may explain the higher maximum precipitation intensities and  $Q_p$  values during  
708 negative MEI conditions in the LCRB. Strengthening of the NAM may be due in part to  
709 the large temperature difference between the cool sea surface of the eastern Pacific Ocean  
710 and the hot land surface of the southwestern U.S. and northwestern Mexico during La  
711 Niña conditions. The large temperature gradient increases winds inland, bringing the  
712 moisture associated with the NAM (Grantz et al., 2007). In the UCRB it is during  
713 negative MEI conditions, where the highest maximum precipitation intensities and  $Q_p$   
714 values for all recurrence intervals occur. This suggests that the UCRB is affected by  
715 ENSO much like the northwestern U.S., where wetter winters are affiliated with La Niña  
716 and not El Niño conditions (Cayan et al., 1999; Hidalgo and Dracup, 2003). It is  
717 important to note that this comparison is of intensity rates and not total precipitated  
718 moisture so the MEI condition resulting in wetter conditions is not known.

719 In addition to the ENSO analysis, by investigating previous studies we see that,  
720 along with natural yearly precipitation variability, the 1996 to 2004 water years included  
721 many atmospheric river events (Dettinger, 2004; Dettinger et al., 2011). It is important  
722 that these events were included due to their ability to greatly increase winter precipitation  
723 in the UCRB and LCRB (Rutz and Steenburgh, 2012). Atmospheric river events  
724 (sometimes known as Pineapple Express events) can also be tied to major Pacific climate  
725 modes such as the ENSO (Dettinger, 2004; Dettinger, 2011), the Pacific Decadal  
726 Oscillation (PDO; Dettinger, 2004), and the North Pacific Gyre Oscillation (NPGO;  
727 Reheis et al., 2012) in southern California. Unfortunately, correlations between  
728 atmospheric river events are unknown and/or less clear for the interior western U.S.  
729 However, all three of these Pacific climate modes shifted during the 9-year study period  
730 in ~1998 to 1999 (Reheis et al., 2012) indicating that both positive and negative  
731 conditions of the ENSO, PDO, and NPGO exist in the NEXRAD products used in this  
732 study.

733 The presence of distinct trends in maximum precipitation and  $Q_p$  values calculated  
734 for negative and positive MEI conditions, as well as the information in the literature on

735 atmospheric river events, indicates the NEXRAD products used in this study incorporate  
736 circulation-scale weather patterns. In addition, the patterns in maximum precipitation and  
737  $Q_p$  values during different MEI conditions agree with common understanding of the  
738 effects of ENSO on the western U.S. and provide evidence that the data and methods  
739 used in this paper to analyze precipitation are reliable. This analysis shows that the  
740 NEXRAD products worked well in this location and that using radar-derived  
741 precipitation products may be useful for identifying precipitation and climatic trends in  
742 other locations where the FMAC method can be applied.

743

## 744 **6. Conclusions**

745 In this study we present the new FMAC method of calculating precipitation and  
746 flood discharges of a range of recurrence intervals using radar-derived precipitation  
747 estimates combined with a flow-routing algorithm. This method improves on the  
748 traditional FEC by assigning recurrence interval information to each value and/or curve.  
749 Also, instead of relying on stream-gauge records of discharge, this method uses up-to-  
750 date and spatially complete radar-derived precipitation estimates (in this case NEXRAD  
751 products) to calculate flood discharges using flow-routing algorithms. This study presents  
752 an alternative data source and method for flood-frequency analysis by calculating  
753 extreme (high recurrence interval) event magnitudes from a large sample set of  
754 magnitudes made possible by sampling the radar-derived precipitation estimates.

755 The FMACs for  $Q_p$  and  $Q_{fd}$  for the UCRB were similar to those produced for the  
756 LCRB. In general, all recurrence-interval curves followed the same general trend,  
757 indicating that the mechanisms of precipitation and flood discharge are similar for the  
758 two basins. However, there were some differences between the two basins. Overall, there  
759 were larger differences between curves of different recurrence intervals for the UCRB  
760 than the LCRB suggesting a larger range in maximum precipitation intensities, and  
761 therefore  $Q_p$  and  $Q_{fd}$ , in the UCRB relative to the LCRB. For both the UCRB and LCRB  
762 the 50- and 100-year recurrence interval curves for all precipitation and discharge  
763 FMACs were the most similar. This similarity may mean that although historical  
764 discharge records are short, having a 50-year record may not underestimate the 100-year  
765 flood as much as one might expect. Also, for  $Q_p$  and  $Q_{fd}$ , low recurrence-interval values

766 were slightly higher in the LCRB than in the UCRB. This relationship was opposite for  
767 high recurrence-interval values. This likely points to a general hydroclimatic difference  
768 between the two basins, with the LCRB receiving high intensity storms annually due to  
769 the NAM and the UCRB receiving more intense and rarer winter frontal storms.

770 Power-law relationships between maximum precipitation intensity,  $Q_p$ , and  
771 contributing area were also found in this study. Maximum precipitation intensities  
772 decreased as a power-law function of contributing area with an average exponent of  $-0.18$   
773  $\pm 0.06$  for all recurrence intervals.  $Q_p$  values for all recurrence intervals increased as a  
774 power-law function of contributing area with an exponent of approximately  $0.82 \pm 0.06$   
775 on average. Based on the constant power-law relationship between  $Q_p$  and contributing  
776 area, the “gap” or characteristic concave-down shape of published FEC are likely not  
777 caused by precipitation limitations.

778 In general, the FMACs of  $Q_{fd}$  calculated in this study are lower than, and exceed,  
779 the published FECs for the LCRB at lower and higher contributing areas. All FMACs of  
780  $Q_{fd}$  were positioned well below the U.S. FEC except the UCRB 500-year FMAC, which  
781 approximated the U.S. FEC during wet antecedent-moisture conditions. All FMACs of  
782  $Q_{fd}$  for all moisture conditions in the LCRB closely approximated the same magnitudes  
783 as the published LCRB FEC, but exceeded it for larger contributing areas. The higher  
784 estimates of flood discharges at larger contributing areas may be the result of the  
785 difference of sampling methods and are likely not erroneous and may be proved true by  
786 future events.

787 Lastly, the approximately 9 years of NEXRAD products were found to be a good  
788 representation of climate in the CRB. This conclusion was made based on differences in  
789 precipitation between positive and negative ENSO conditions in both the UCRB and  
790 LCRB and additional data found in the literature. In general, the UCRB was found to  
791 have a hydroclimatic regime much like that of the northwestern U.S. where El Niño  
792 conditions result in lower maximum precipitation intensities and amounts and La Niña  
793 conditions result in higher maximum precipitation intensities. The LCRB showed a more  
794 complex trend with similar maximum precipitation intensities for both El Niño and La  
795 Niña conditions.

796           Here this method is applied to the UCRB and LCRB in the southwestern U.S., but  
797 could be applied to other regions of the U.S. and the world with variable climate and  
798 storm types where radar-derived precipitation estimates are available. In addition, this  
799 study used set values of contributing area, drainage basin shape, time intervals of  
800 measurement, and recurrence intervals that can be changed based on the focus of future  
801 studies. Other variables such as snowpack, elevation, and land use should be explored in  
802 conjunction with this method to better understand controls on precipitation and flooding.

803

#### 804 **Acknowledgments**

805           This study was supported by the Jemez River Basin and Santa Catalina Critical  
806 Zone Observatory NSF grants EAR-0724958 and EAR-1331408. We would like to thank  
807 Vic Baker, Phil Pearthree, Peter Troch, and Katie Hirschboeck for helpful discussions  
808 and suggestions.

809 **References**

- 810 Baeck, M.L. and Smith, J.A.: Rainfall estimates by the WSR-88D for heavy rainfall  
811 events, *Weather Forecast.*, 13, 416-436, 1998.  
812
- 813 Baker, V.R.: Paleoflood hydrology and extraordinary flood events, *J. Hydrol.*, 96, 77-99,  
814 1987.  
815
- 816 Brutsaert, W.: Review of Green's functions for linear open channels, *J. Eng. Mech.-*  
817 *ASCE*, 99, 1247-1257, 1973.  
818
- 819 Burton, G.A., Jr. and Pitt, R.E (Eds.): *Stormwater effects handbook: a toolbox for*  
820 *watershed managers, scientists, and engineers*, Lewis Publishers, Boca Raton, Florida,  
821 2001.  
822
- 823 Cañon, J., González, J., and Valdes, J.: Precipitation in the Colorado River Basin and its  
824 low frequency associations with PDO and ENSO signals, *J. Hydrol.*, 333, 252-264, 2007.  
825
- 826 Castellarin, A.: Probabilistic envelope curves for design flood estimation at ungauged  
827 sites, *Water Resour. Res.*, 43, W04406, doi:10.1029/2005WR004384, 2007.  
828
- 829 Castellarin, A., Vogel, R.M., and Matalas, N.C.: Probabilistic behavior of a regional  
830 envelope curve, *Water Resour. Res.*, 41, W06018, doi:10.1029/2004WR003042, 2005.  
831
- 832 Castellarin, A., Merz, R., and Blöschl, G.: Probabilistic envelope curves for extreme  
833 rainfall events, *J. Hydrol.*, 378, 263-271, 2009.  
834
- 835 Castro, C.L., McKee, T.B., and Pielke, R.A. Sr.: The relationship of the North American  
836 Monsoon to Tropical and North Pacific surface temperatures as revealed by observational  
837 analyses, *J. Climate*, 14, 4449-4473, 2001.  
838



839 Cayan, D.R., Redmond, K.T., and Riddle, L.G.: ENSO and hydrologic extremes in the  
840 western United States, *J. Climate*, 12, 2881-2893, 1999.  
841

842 Costa, J.E.: A comparison of the largest rainfall-runoff floods in the United States with  
843 those of the People's Republic of China and the World, *J. Hydrol.*, 96, 101-115, 1987.  
844

845 Crippen, J.R. and Bue, C.D.: Maximum flood flows in the conterminous United States,  
846 U.S. Geological Survey Water Supply Paper 1887, 1977.  
847

848 Dettinger, M.: Fifty-two years of "Pineapple-Express" storms across the west coast of  
849 North America, U.S. Geological Survey, Scripps Institution of Oceanography for the  
850 California Energy Commission, PIER Energy-Related Environmental Research, CEC-  
851 500-2005-004, 2004.  
852

853 Dettinger, M.D., Ralph, F.M., Das, T., Neiman, P.J., and Cayan, D.R.: Atmospheric  
854 rivers, floods, and the water resources of California, *Water*, 3, 445-478, 2011.  
855

856 Enzel, Y., Ely, L.L., House, P.K., Baker, V.R., and Webb, R.H.: Paleoflood evidence for  
857 a natural upper bound to flood magnitudes in the Colorado River Basin, *Water Resour.*  
858 *Res.*, 29, 2287-2297, 1993.  
859

860 Etheredge, D., Gutzler, D.S., and Pazzaglia, F.J.: Geomorphic response to seasonal  
861 variations in rainfall in the Southwest United States, *Geol. Soc. Am. Bull.*, 116, 606-618,  
862 2004.  
863

864 Federal Emergency Management Agency: Modernizing FEMA's flood hazard mapping  
865 program: Recommendations for using future-conditions hydrology for the National Flood  
866 Insurance Program, Final Report, U.S. Department of Homeland Security, 2001.  
867

868 Fulton, R.A., Breidenbach, J.P., Seo, D.J., Miller, D.A., and O'Bannon, T.: The WSR-  
869 88D algorithm, *Weather Forecast.*, 13, 377-395, 1998.

870

871 Giannoni, F., Smith, J.A., Zhang, Y., and Roth, G., 2003: Hydrologic modeling of  
872 extreme floods using radar rainfall estimates, *Adv. Water Resour.*, 26, 195-203, 2003.

873

874 Grantz, K., Rajagopalan, B., Clark, M., and Zagona, E.: Seasonal shifts in the North  
875 American Monsoon, *J. Climate*, 20, 1923-1935, 2007.

876

877 [Henderson, F.M.: Some properties of the unit hydrograph, \*J. Geophys. Res.\*, 68, 4785-](#)  
878 [4793, 1963.](#)

879

880 Herschy, R.: The world's maximum observed floods, *Flow Meas. Instrum.*, 13, 231-235,  
881 2002.

882

883 Hidalgo, H.G. and Dracup, J.A.: ENSO and PDO Effects on hydroclimatic variations of  
884 the Upper Colorado River Basin, *J. Hydrometeorol.*, 4, 5-23, 2003.

885

886 House, P.K. and Hirschboeck, K.K.: Hydroclimatological and paleohydrological context  
887 of extreme winter flooding in Arizona, 1993, in: Larson, R.A. and Slosson, J.E. (Eds.),  
888 Storm-Induced Geologic Hazards: Case Histories from the 1992-1993 Winter in Southern  
889 California and Arizona, Geological Society of America Reviews in Engineering Geology,  
890 vol. XI, Boulder, Colorado, 1-24, 1997.

891

892 Johnson, D., Smith, M., Koren, V., and Finnerty, B.: Comparing mean areal precipitation  
893 estimates from NEXRAD and rain gauge networks, *J. Hydrol. Eng.*, 4, 117-124, 1999.

894

895 Kang, K. and Merwade, V.: Development and application of a storage-release based  
896 distributed hydrologic model using GIS, *J. Hydrol.*, 403, 1-13, 2011.

897

898 Li, Bai: Current status of weather radar data exchange, World Meteorological  
899 Organization Workshop on Radar Data Exchange, Exeter, UK, April 2013, 16.IV.2013,

900 | 2013.

901  
902  
903  
904  
905  
906  
907  
908  
909  
910  
911  
912  
913  
914  
915  
916  
917  
918  
919  
920  
921  
922  
923  
924  
925  
926  
927  
928  
929  
930

[Marani, M., Rinaldo, A., Rigon, R., Rodriguez-Iturbe, I.: Geomorphological width functions and the random cascade, Geophys. Res. Lett., 21, 2123-2126, 1994.](#)

Mesa, O.J. and Mifflin, E.R.: On the relative role of hillslope and network geometry in hydrologic response, in: Gupta, V.K., Rodriguez-Iturbe, I., and Wood, E.F., (Eds.), Scale Problems in Hydrology, D. Reidel, Dordrecht, Netherlands, 1-17, 1986.

Miller, A.J.: Flood hydrology and geomorphic effectiveness in the central Appalachians, Earth Surf. Processes, 15, 119-134, 1990.

Milly, P.C.D., Betancourt, J., Falkenmark, M., Hirsch, R.M., Kundzewicz, Z.W., Lettenmaier, D.P., and Stouffer, R.J.: Stationarity is dead: Whither water management?, Science, 319, 573-574, 2008.

Moody, T., Wirtanen, M., Yard, S.N.: Regional relationships for bankfull stage in natural channels of the arid southwest, National Channel Design Inc., Flagstaff, AZ, 38 pp., 2003.

Morrison, J.E. and Smith, J.A.: Stochastic modeling of flood peaks using the generalized extreme value distribution, Water Resour. Res., 38(12), 1305  
doi:10.1029/2001WR000502, 2002.

Moussa, R.: What controls the width function shape, and can it be used for channel network comparison and regionalization?, Water Resour. Res., 44, W08456,  
doi:10.1029/2007WR006118, 2008.

National Atlas: <http://www.nationalatlas.gov/atlasftp.html#hucs00m>, last access: 8 August 2014

931 | [Niezgoda, S. and West, T. \(2012\) Relationships between Watershed and Stream](#)  
932 | [Characteristics and Channel Forming Discharge in Snowmelt Dominated Streams. World](#)  
933 | [Environmental and Water Resources Congress 2012: pp. 1575-1584.](#)  
934 | [doi: 10.1061/9780784412312.157](#)  
935 |  
936 | NOAA HDSG: [http://dipper.nws.noaa.gov/hdsb/data/nexrad/cbrfc\\_stageiii.php](http://dipper.nws.noaa.gov/hdsb/data/nexrad/cbrfc_stageiii.php), last  
937 | access: 8 August 2014.  
938 |  
939 | Ogden, F.L. and Julien, P.Y.: Runoff model sensitivity to radar rainfall resolution, J.  
940 | Hydrol., 158, 1-18, 1994.  
941 |  
942 | Parrett, C. and Johnson, D.R.: Methods for estimating flood frequency in Montana based  
943 | on data through water year 1998, U.S. Geological Survey Water-Resources Investigations  
944 | Report 03-4308, 2003.  
945 |  
946 | Parzen, E.: Nonparametric statistical data modeling, J. Am. Statist. Assoc., 74, 365, 105-  
947 | 121, 1979.  
948 |  
949 | [Puente, C.E. and Sivakumar, B.: A deterministic width function model, Nonlinear Proc.](#)  
950 | [Geoph., 10, 525-529, 2004.](#)  
951 |  
952 | RadarEU: <http://www.radareu.cz/>, last access 1 August, 2014.  
953 |  
954 | Reed, S.M. and Maidment, D.R.: Coordinate transformations for using NEXRAD data in  
955 | GIS-based hydrologic modeling, J. Hydrol. Eng., 4, 174-182, 2006.  
956 |  
957 | Reheis, M.C., Bright, J., Lund, S.P., Miller, D.M., Skipp, G., and Fleck, R.J.: A half-  
958 | million-year record of paleoclimate from the Lake Manix Core, Mojave Desert,  
959 | California, Palaeogeogr. Palaeoclimatol., 365-366, 11-27, 2012.  
960 |

961 Rinaldo, A., Marani, A., and Rigon, R.: Geomorphological dispersion, *Water Resour.*  
962 *Res.*, 27, 513-525, 1991.

963 |

964 [Rinaldo, A., Vogel, G.K., Rigon, R., Rodriguez-Itrube, I.: Can one gauge the shape of a](#)  
965 [basin?, \*Water Resour. Res.\*, 31, 1119-1127, 1995.](#)

966

967 Rodriguez-Iturbe, I. and Valdes, J.B.: The geomorphic structure of hydrologic response,  
968 *Water Resour. Res.*, 15, 1409-1420, 1979.

969

970 Rosenburg, E.A., Clark, E.A., Steinemann, A.C., and Lettenmaier, D.P.: On the  
971 contribution of groundwater storage to interannual streamflow anomalies in the Colorado  
972 River basin, *Hydrol. Earth Sys. Sc.*, 17, 1475-1491, 2013.

973

974 Rutz, J.J. and Steenburgh, W.J.: Quantifying the role of atmospheric rivers in the interior  
975 western United States, *Atmos. Sci. Lett.*, 13, 257-261, doi:10.1002/asl.392, 2012.

976

977 Saco, P.M. and Kumar, P.: Kinematic dispersion effects of hillslope velocities, *Water*  
978 *Resour. Res.*, 40, W01301, doi:10.1029/2003WR002024, 2004.

979

980 Sankarasubramanian, A. and Vogel, R.M.: Hydroclimatology of the continental United  
981 States, *Geophys. Res. Lett.*, 30, 1363, doi:10.1029/2002GL015937, 2003.

982

983 Shedd, R.C. and Fulton, R.A.: WSR-88D precipitation processing and its use in National  
984 Weather Service hydrologic forecasting, in: *Proceedings, Engineering Hydrology:*  
985 *Proceedings of the Symposium Sponsored by the Hydrology Division of American*  
986 *Society of Civil Engineers*, 844-848, 1993.

987

988 Sivapalan, M. and Blöschl, G.: Transformation of point rainfall to areal rainfall:  
989 Intensity-duration-frequency curves, *J. Hydrol.*, 204, 150-167, 1998.

990

991 Smith, J.A. and Krajewski, W.F.: A modeling study of rainfall rate-reflectivity  
992 relationships, *Water Resour. Res.*, 29, 2505-2514, 1993.  
993  
994 Smith, J.A., Seo, D.J., Baeck, M.L., and Hudlow, M.D.: An intercomparison study of  
995 NEXRAD precipitation data, *Water Resour. Res.*, 32, 2035-2045, 1996.  
996  
997 Troch, P.A., Smith, J.A., Wood, E.F., and de Troch, F.P.: Hydrologic controls of large  
998 floods in a small basin: central Appalachian case study, *J. Hydrol.*, 156, 285-309, 1994.  
999  
1000 [Veneziano, D., Moglen, G.E., Furcolo, P., Iacobellis, V.: Stochastic model of the width](#)  
1001 [function, \*Water Resour. Res.\*, 36, 1143-1157, 2000.](#)  
1002  
1003 Vivoni, E.R., Entekhabi, D., Bras, R.L., and Ivanov, V.Y.: Controls on runoff generation  
1004 and scale-dependence in a distributed hydrologic model, *Hydrol. Earth Sys. Sc.*, 4, 983-  
1005 1029, 2007.  
1006  
1007 Vogel, R.M., and Fenneset, N.M., Flow-duration curves I: New interpretation and  
1008 confidence intervals, *J. Water Resour. Bull.*, 31, 6, 485-504, 1994.  
1009  
1010 Wolman, M.G. and Costa, J.E.: Envelope curves for extreme flood events, *J. Hydraul.*  
1011 *Eng.-ASCE, Discussion*, 110, 77-78, 1984.  
1012  
1013 Xie, H., Zhou, X., Hendricks, J.M.H., Vivoni, E.R., Guan, H., Tian, Y.Q., and Small,  
1014 E.E.: Evaluation of Nexrad Stage III precipitation data over a semiarid region, *J. Am.*  
1015 *Water Resour. As.*, 04055, 237-256, 2006.  
1016  
1017  
1018  
1019  
1020  
1021

1022 **Tables**

1023 Table 1. Maximum precipitation intensity and  $Q_p$  for the Upper Colorado River Basin  
 1024 (UCRB) and Lower Colorado River Basin (LCRB). Note that data are all sampled from  
 1025 time intervals of measurement  $\leq 2$  hours.

<u>RI</u>	<u>Area</u> <u>(km<sup>2</sup>)</u>	<u>Intensity</u> <u>(mm h<sup>-1</sup>)</u>		<u><math>Q_p</math></u> <u>(m<sup>3</sup> s<sup>-1</sup>)</u>	
		<u>UCRB</u>	<u>LCRB</u>	<u>UCRB</u>	<u>LCRB</u>
<u>10</u>	<u>16</u>	<u>28.0 ± 0.0</u>	<u>36.6 ± 0.0</u>	<u>125 ± 0</u>	<u>162 ± 0</u>
<u>10</u>	<u>64</u>	<u>25.4 ± 0.1</u>	<u>32.5 ± 0.0</u>	<u>451 ± 1</u>	<u>578 ± 0</u>
<u>10</u>	<u>144</u>	<u>25.1 ± 1.1</u>	<u>29.5 ± 0.4</u>	<u>1004 ± 44</u>	<u>1182 ± 16</u>
<u>10</u>	<u>256</u>	<u>23.7 ± 0.2</u>	<u>27.3 ± 0.0</u>	<u>1682 ± 13</u>	<u>1944 ± 1</u>
<u>10</u>	<u>1024</u>	<u>19.8 ± 1.5</u>	<u>19.7 ± 0.4</u>	<u>5644 ± 427</u>	<u>5610 ± 114</u>
<u>10</u>	<u>1296</u>	<u>20.7 ± 2.4</u>	<u>21.7 ± 3.5</u>	<u>7439 ± 873</u>	<u>7820 ± 1268</u>
<u>10</u>	<u>4096</u>	<u>15.5 ± 3.0</u>	<u>15.9 ± 0.8</u>	<u>17682 ± 3462</u>	<u>18134 ± 890</u>
<u>10</u>	<u>11664</u>	<u>12.6 ± 1.7</u>	<u>11.0 ± 2.6</u>	<u>40914 ± 5571</u>	<u>35521 ± 8586</u>
<u>50</u>	<u>16</u>	<u>55.9 ± 0.7</u>	<u>56.2 ± 0.1</u>	<u>248 ± 3</u>	<u>250 ± 0</u>
<u>50</u>	<u>64</u>	<u>55.1 ± 1.2</u>	<u>47.7 ± 0.0</u>	<u>980 ± 22</u>	<u>847 ± 1</u>
<u>50</u>	<u>144</u>	<u>55.3 ± 3.5</u>	<u>43.3 ± 0.9</u>	<u>2211 ± 142</u>	<u>1734 ± 38</u>
<u>50</u>	<u>256</u>	<u>54.9 ± 1.4</u>	<u>40.9 ± 0.5</u>	<u>3901 ± 101</u>	<u>2908 ± 32</u>
<u>50</u>	<u>1024</u>	<u>50.8 ± 5.5</u>	<u>33.6 ± 1.4</u>	<u>14449 ± 1569</u>	<u>9560 ± 393</u>
<u>50</u>	<u>1296</u>	<u>50.8 ± 25.0</u>	<u>32.5 ± 3.9</u>	<u>18287 ± 9011</u>	<u>11704 ± 1410</u>
<u>50</u>	<u>4096</u>	<u>27.6 ± 22.2</u>	<u>30.0 ± 5.2</u>	<u>31382 ± 25313</u>	<u>34126 ± 5969</u>
<u>50</u>	<u>11664</u>	<u>21.1*</u>	<u>15.4 ± 8.3</u>	<u>68434*</u>	<u>49764 ± 26874</u>
<u>100</u>	<u>16</u>	<u>92.3 ± 0.3</u>	<u>68.6 ± 0.0</u>	<u>410 ± 1</u>	<u>305 ± 0</u>
<u>100</u>	<u>64</u>	<u>91.9 ± 2.5</u>	<u>54.5 ± 0.2</u>	<u>1635 ± 44</u>	<u>970 ± 3</u>
<u>100</u>	<u>144</u>	<u>90.1 ± 3.0</u>	<u>51.9 ± 1.0</u>	<u>3606 ± 118</u>	<u>2075 ± 41</u>
<u>100</u>	<u>256</u>	<u>88.7 ± 4.3</u>	<u>48.4 ± 0.4</u>	<u>6305 ± 307</u>	<u>3440 ± 27</u>
<u>100</u>	<u>1024</u>	<u>63.8 ± 11.0</u>	<u>42.5 ± 2.2</u>	<u>18155 ± 3139</u>	<u>12085 ± 630</u>
<u>100</u>	<u>1296</u>	<u>78.5 ± 50.1</u>	<u>43.2 ± 7.8</u>	<u>28257 ± 18022</u>	<u>15544 ± 2820</u>
<u>100</u>	<u>4096</u>	<u>40.8*</u>	<u>32.0 ± 10.4</u>	<u>46422*</u>	<u>36425 ± 11803</u>
<u>100</u>	<u>11664</u>	<u>21.1*</u>	<u>20.1*</u>	<u>68434*</u>	<u>65011*</u>
<u>500</u>	<u>16</u>	<u>254.0 ± 0.8</u>	<u>81.9 ± 0.5</u>	<u>1129 ± 3</u>	<u>364 ± 2</u>
<u>500</u>	<u>64</u>	<u>229.0 ± 3.1</u>	<u>68.6 ± 1.5</u>	<u>4071 ± 55</u>	<u>1219 ± 26</u>
<u>500</u>	<u>144</u>	<u>219.1 ± 11.9</u>	<u>68.6 ± 4.7</u>	<u>8762 ± 476</u>	<u>2743 ± 187</u>
<u>500</u>	<u>256</u>	<u>219.4 ± 7.3</u>	<u>68.6 ± 3.4</u>	<u>15600 ± 517</u>	<u>4877 ± 242</u>
<u>500</u>	<u>1024</u>	<u>166.0 ± 44.1</u>	<u>68.6 ± 3.1</u>	<u>47229 ± 12554</u>	<u>19507 ± 884</u>
<u>500</u>	<u>1296</u>	<u>174.6 ± 85.3</u>	<u>65.6 ± 31.3</u>	<u>62862 ± 30696</u>	<u>23624 ± 11279</u>
<u>500</u>	<u>4096</u>	<u>81.6*</u>	<u>53.6*</u>	<u>92844*</u>	<u>60930*</u>
<u>500</u>	<u>11664</u>	<u>21.1*</u>	<u>20.1*</u>	<u>68434*</u>	<u>65011*</u>

1026 \* Values with infinite confidence intervals, not used in this study.

1027

1028

1029

1030

1031

1032 Table 2. Maximum  $Q_{fd}$  for the Upper Colorado River Basin (UCRB) and Lower Colorado  
 1033 River Basin (LCRB). Note that data are all sampled from time intervals of measurement  
 1034  $\leq 2$  hours.

RI	Area (km <sup>2</sup> )	Wet $Q_{fd}$ (m <sup>3</sup> s <sup>-1</sup> )		Med $Q_{fd}$ (m <sup>3</sup> s <sup>-1</sup> )		Dry $Q_{fd}$ (m <sup>3</sup> s <sup>-1</sup> )	
		UCRB	LCRB	UCRB	LCRB	UCRB	LCRB
10	16	65 ± 0	86 ± 0	36 ± 0	47 ± 0	20 ± 0	26 ± 0
10	64	246 ± 1	263 ± 0	137 ± 0	151 ± 0	75 ± 0	89 ± 0
10	144	465 ± 20	489 ± 7	268 ± 12	290 ± 4	156 ± 7	175 ± 2
10	256	657 ± 5	748 ± 0	388 ± 3	449 ± 0	244 ± 2	283 ± 0
10	1024	2363 ± 179	2194 ± 44	1423 ± 108	1326 ± 27	892 ± 68	820 ± 17
10	1296	2244 ± 263	2384 ± 387	1459 ± 171	1543 ± 250	1010 ± 118	1066 ± 173
10	4096	5594 ± 1095	5304 ± 260	3665 ± 718	3375 ± 166	2507 ± 491	2315 ± 114
10	11664	14603 ± 1966	11048 ± 2670	9010 ± 1213	6978 ± 1687	6105 ± 822	4942 ± 1195
50	16	131 ± 2	131 ± 0	73 ± 1	73 ± 0	41 ± 1	41 ± 0
50	64	553 ± 12	387 ± 0	307 ± 7	222 ± 0	172 ± 4	130 ± 0
50	144	1145 ± 73	720 ± 16	636 ± 41	424 ± 9	355 ± 23	259 ± 6
50	256	1772 ± 46	1119 ± 12	1043 ± 27	676 ± 7	639 ± 16	421 ± 5
50	1024	6127 ± 665	3062 ± 126	3665 ± 398	1928 ± 79	2291 ± 249	1308 ± 54
50	1296	7076 ± 3487	3562 ± 429	4265 ± 2102	2300 ± 277	2682 ± 1321	1571 ± 189
50	4096	15716 ± 12650	8487 ± 1485	9451 ± 7607	5850 ± 1023	6076 ± 4890	4343 ± 760
50	11664	44482*	15700 ± 8478	28783*	10176 ± 5495	19770*	7138 ± 3855
100	16	216 ± 1	160 ± 0	120 ± 0	89 ± 0	67 ± 0	50 ± 0
100	64	924 ± 25	442 ± 1	514 ± 14	255 ± 1	286 ± 8	150 ± 0
100	144	1807 ± 60	860 ± 17	1041 ± 35	508 ± 10	610 ± 20	309 ± 6
100	256	2888 ± 140	1324 ± 10	1706 ± 83	798 ± 6	1037 ± 50	499 ± 4
100	1024	10586 ± 1830	3812 ± 199	6366 ± 1101	2438 ± 127	3979 ± 688	1662 ± 87
100	1296	9564 ± 6100	4713 ± 855	5752 ± 3668	3058 ± 555	3619 ± 2308	2104 ± 382
100	4096	29415*	10319 ± 3344	19095*	6654 ± 2156	13116*	4698 ± 1522
100	11664	59600*	18607*	38667*	12904*	26747*	9609*
500	16	594 ± 2	192 ± 1	330 ± 1	107 ± 1	184 ± 1	59 ± 0
500	64	1855 ± 25	556 ± 12	1068 ± 14	320 ± 7	628 ± 8	188 ± 4
500	144	3631 ± 197	1138 ± 77	2141 ± 116	670 ± 46	1306 ± 71	408 ± 28
500	256	6012 ± 200	1879 ± 93	3618 ± 120	1130 ± 56	2266 ± 75	709 ± 35
500	1024	19049 ± 5059	6139 ± 278	11478 ± 3048	3945 ± 179	7186 ± 1909	2660 ± 120
500	1296	19075 ± 9314	7153 ± 3415	12370 ± 6041	4656 ± 2223	8499 ± 4150	3198 ± 1527
500	4096	43688*	14892*	28354*	10460*	19481*	7800*
500	11664	65705*	23062*	42738*	16198*	29364*	12080*

1035 \* Values with infinite confidence intervals, not used in this study.

1036

1037

1038

1039

1040

1041

1042

1043



1044 Table 3. Maximum precipitation intensity and  $Q_p$  values for 10, 50, 100, and 500-year  
 1045 recurrence intervals during negative (neg) and positive (pos) Multivariate ENSO Index  
 1046 (MEI) conditions within the Lower Colorado River Basin (LCRB) and Upper Colorado  
 1047 River Basin (UCRB). Note that data are all sampled from time intervals of measurement  
 1048  $\leq 2$  hours.

Basin	MEI	Area (km <sup>2</sup> )	Intensity (mm h <sup>-1</sup> )				$Q_p$ (m <sup>3</sup> s <sup>-1</sup> )			
			10 yr	50 yr	100 yr	500 yr	10 yr	50 yr	100 yr	500 yr
LCRB	neg	16	39	56	69	77	175	250	305	343
	neg	256	31	46	53	69	2206	3251	3741	4877
	neg	4096	21	32	43	54	23856	36425	48363	60930
	pos	16	40	64	74	130	179	284	330	576
	pos	256	27	38	47	52	1943	2690	3369	3721
	pos	4096	13	20*	20*	20*	15229	22689*	22689*	22689*
UCRB	neg	16	41	98	162	254	186	435	721	1129
	neg	256	33	101	155	254	2366	7172	11012	18055
	neg	4096	22	34	41	82	25556	39013	46422	92844
	pos	16	26	51	56	74	115	225	248	330
	pos	256	18	40	51	56	1255	2810	3601	4018
	pos	4096	10	26	27*	27*	10822	30034	31044*	31044*

1049 \* Values with infinite confidence intervals, not used in this study.

1050

1051

1052

1053

1054

1055

1056

1057

1058

1059

1060

1061

1062

1063

1064

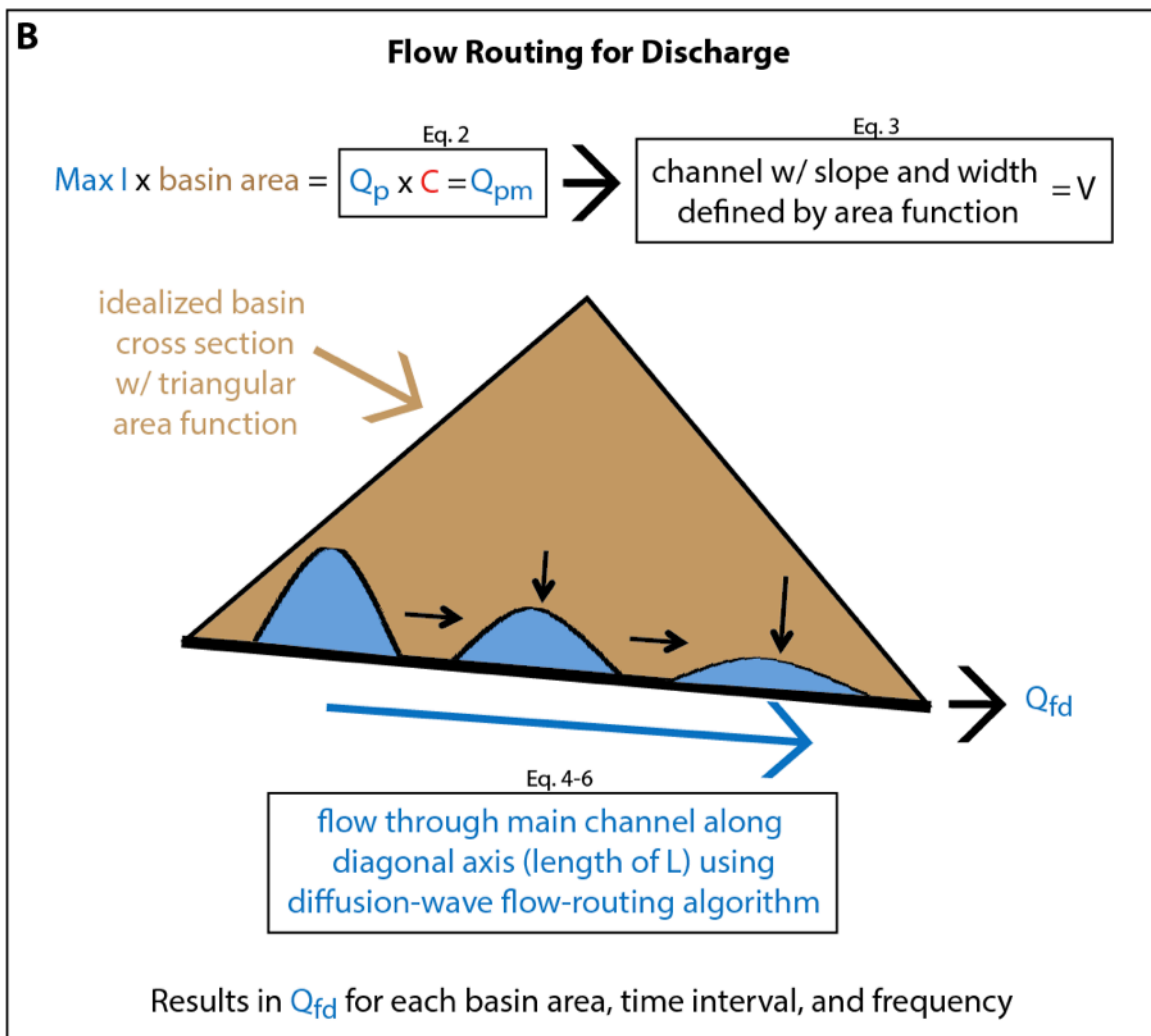
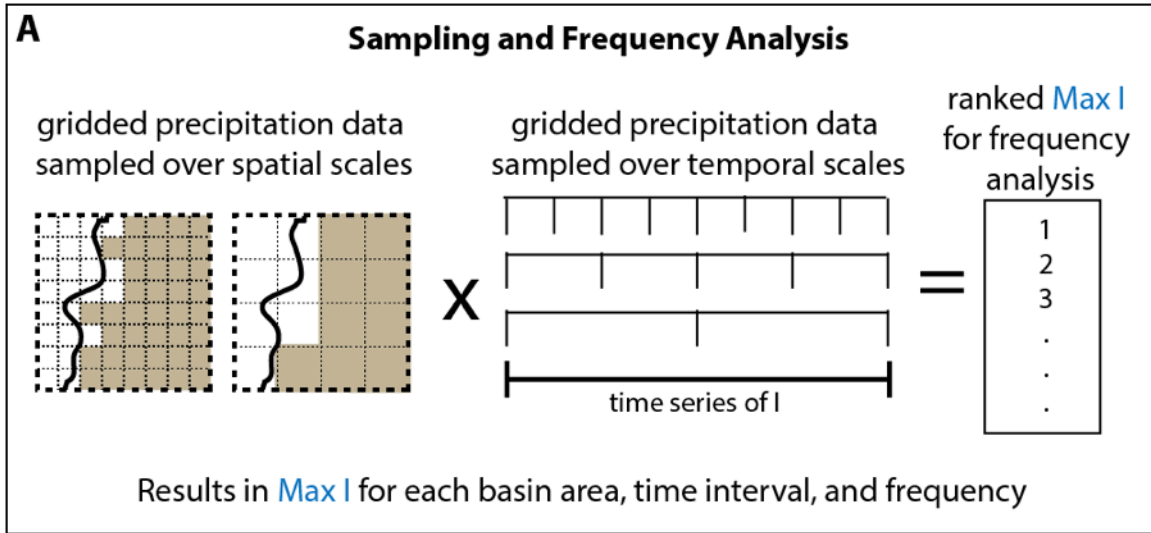
1065

1066 **Figures**

1067

1068 Figure 1. Map showing the locations of the Upper and Lower Colorado River Basins

1069 (UCRB and LCRB, respectively) outlined by the dotted line.



1070

1071

1072

Figure 2. Schematic diagram of methodology used in this paper. (A) Rainfall data is sampled over spatial and temporal scales in factors of two. This sampling does not only

1073 include looking at the data within a given spatial or temporal scale, but aggregating it  
1074 over that scale. These values are ranked for a given basin area and time interval to  
1075 complete the frequency analysis. This results in rainfall intensities (I) for each spatial  
1076 scale (basin area), temporal scale (time interval or storm duration), and frequency. (B)  
1077 Intensities sampled from the rainfall data are used to calculate rainfall discharge ( $Q_p$  and  
1078  $Q_{pm}$ ) values that are then put through the flow routing algorithm in order to calculate  
1079 flood discharge ( $Q_{fd}$ ) values.  $Q_{fd}$  values are then used to construct the frequency-  
1080 magnitude-area curves (FMACs) showing the data for recurrence intervals of 10, 50, 100,  
1081 and 500 years.

1082

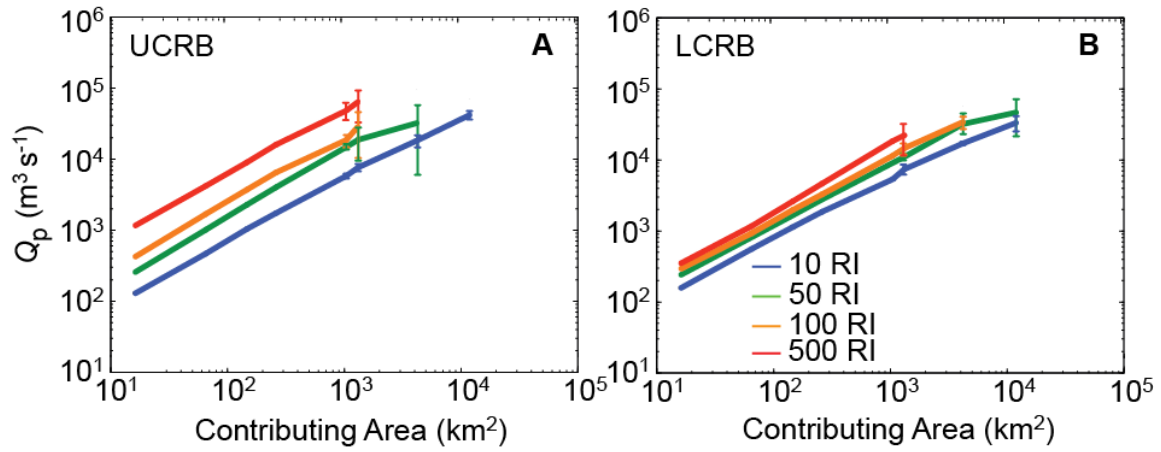
1083 Figure 3. Logarithmic relationships between runoff coefficients and contributing area  
1084 using modeled data for wet (filled diamonds), medium (open squares), and dry (filled  
1085 circles) antecedent-moisture conditions (Vivoni et al., 2007) and measured data for larger  
1086 contributing areas (filled squares; Rosenberg et al., 2013). The medium (open squares)  
1087 and dry (filled circles) data separate into two distinct groups relating to the precipitation  
1088 event used to model them, with the lower group and higher group relating to a 12-h, 1-  
1089 mm h<sup>-1</sup> event and 1-h, 40-mm h<sup>-1</sup> event, respectively. All points were used in the least-  
1090 squares weighed-regression analysis.

1091

1092 Figure 4. Power-law relationships between channel slope and contributing area (A) and  
1093 channel width and contributing area (B) for the Colorado River Basin.

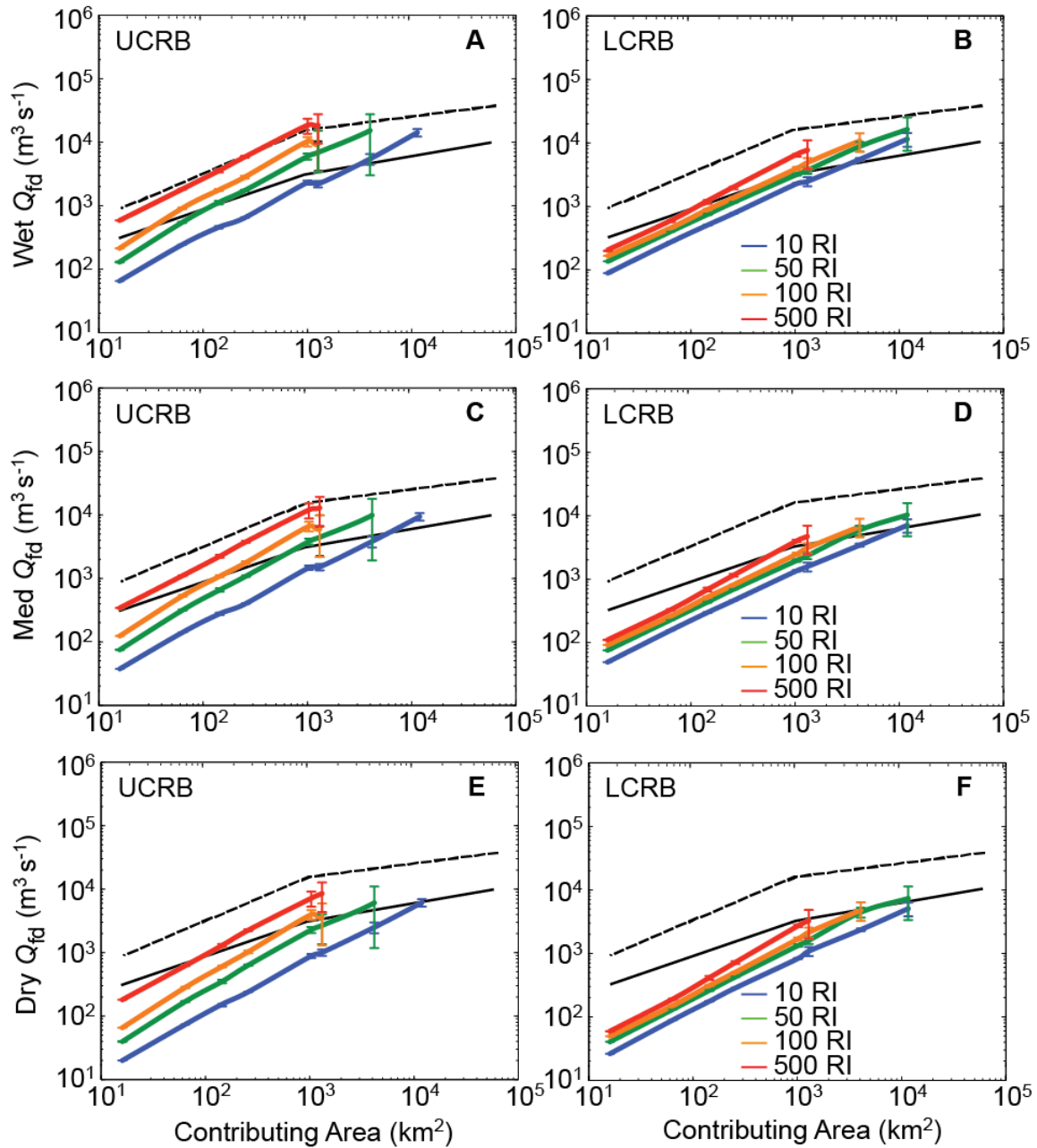
1094

1095 Figure 5. Multivariate ENSO Index (MEI) of months included in Stage III NEXRAD  
1096 gridded products. Months are numbered from September 1996 to September 2005 with  
1097 years shown in gray. Dashed black line MEI equal to zero. Positive MEI indicates El  
1098 Niño conditions, while negative MEI indicates La Niña conditions.



1099

1100 Figure 6. Frequency-magnitude-area (FMA) curves of  $Q_p$  versus contributing area for  
 1101 recurrence intervals (RI) of 10, 50, 100, and 500 years for the Upper Colorado River  
 1102 Basin (UCRB; A) and the Lower Colorado River Basin (LCRB; B).



1103

1104 Figure 7.  $Q_{fd}$  frequency-magnitude-area curves of 10, 50, 100, and 500 recurrence  
 1105 intervals (RI) and for wet, medium, and dry conditions for the Upper Colorado River  
 1106 Basin (UCRB) and the Lower Colorado River Basin (LCRB). Published FECs (black  
 1107 lines) for the Lower Colorado River Basin (solid black line) from Enzel et al. (1993) and  
 1108 the United States (dashed black line) from Costa (1987) are also shown.

1109

1110 Figure 8. Conceptual diagram of the characteristic concave-down shape of the FEC  
1111 (observed) shown in comparison to a power-law function between  $Q_p$  and contributing  
1112 area. The “gap” between the observed curve and the predicted power law is caused by  
1113 precipitation limitations and mechanisms occurring during the routing of water over the  
1114 landscape.  
1115  
1116